A Numeric Integration Program to Simulate Nonlinear QED Processes in Electron-Laser or Photon-Laser Collisions

Christian Bula

Joseph Henry Laboratories, Princeton University,
Princeton, New Jersey 08544

June 1997, Version 1.0

(this is file /afs/slac/www/exp/e144/ps/nidoc.ps)

Abstract

This document describes a program to simulate nonlinear QED processes in collisions between a cylindrical electron or photon beam with a focused, high intensity laser pulse. The simulated processes are nonlinear Compton scattering, multiphoton Breit-Wheeler and multiphoton trident pair production in a circularly or linearly polarized laser field. The yield and spectra of final state particles are calculated by numerically integrating the differential reaction rates for these processes over space and time in the beam-laser interaction region. The program allows for an interaction geometry that includes an arbitrary crossing angle between the two beams as well as a not diffraction limited focal spot for the laser beam. Variations of the effective crossing angle between laser photons and beam particles introduced by the focused laser beam are taken into account. Also, the attenuation of the particle beam as it passes through the laser field is included in the simulation. In addition to calculating the final states of primary beam-laser interactions, the program also simulates further (secondary) interactions between the reaction products and the laser field. The speed of the simulation was a major concern in the program development and several methods to reduce the required CPU time are presented. The document concludes with a detailed description of source files, program options, input parameters and instructions for program installation and setup.

Contents

List of Figures

1 Introduction

The numeric integration program (NI) described in this document was developed to simulate nonlinear QED processes in the collision between a high-energy electron or photon beam and an intense laser pulse. These processes are measured by the E-144 collaboration in an experiment at the Final Focus Test Beam (FFTB) at SLAC. The method used in this simulation is a numeric integration of differential reaction rates over both space and time in the beam-laser interaction region.

In a Monte-Carlo approach to a strong-field QED simulation (as implemented for example in the ABEL program), individual particles are tracked in small steps through the laser field. At each step, the program calculates the probabilities for several possible interactions and then makes a decision, based on a pseudo random number, whether an interaction occurs. In order to calculate all possible reaction types with statistically significant precision, this procedure must be repeated many times.

In a numerical integration as described here, space and time are divided in small elements and reaction yields are calculated for each of these elements. The calculations for a space-time elements are based on particle densities (and not single particles) and one tries to account for all possible interactions at once by multiplying particle densities with reaction probabilities. Finally, the results for all elements are combined.

Of course, both methods have their advantages and disadvantages. Usually, a Monte-Carlo program is more flexible and second order corrections are easier to implement. In addition, it allows to keep a history of interactions for each particle in the simulation. On the other hand, a numeric integration is usually faster and free of statistical fluctuations.

The main goal of NI was to have a fast, flexible and easy-to-use tool to reliably predict reaction rates and energy spectra of photons, electrons and positrons originating at the two interaction points planed for the E-144 experiment, *i.e.* an electron-laser interaction point (IP1) and a photon-laser interaction point (IP2). The simulation should also take into account the correct interaction geometry, *e.g.* a crossing angle between the beam and the laser pulse or a temporal or spatial offset between the two pulses.

The calculation for IP1 required the simulation of nonlinear Compton scattering between monoenergetic beam electrons and laser photons in a first step. However, since the scattered electrons and the backscattered photons may still be inside the laser field at the scattering point, further interactions had to be considered. The electrons may undergo further Compton scatters and the photons may produce electron-positron pairs by absorption of several laser photons. Furthermore, the positrons and electrons from pair creation are again subject to Compton scattering until they leave the laser field. Results from the IP1 simulation were used to plan and optimize detector positions and adjust amplifier gains prior to data-taking runs, as well as to compare the experimental data with theory.

So far, photon-laser collisions at IP2 have not been realized experimentally, and therefore a lesser effort was made to achieve a realistic simulation of this experiment. The current simulation supports three options for the photon beam, namely a monoenergetic spectrum (unrealistic but easy to implement), a bremsstrahlung spectrum (foil at IP1) or the spectrum from nonlinear Compton scattering (laser at IP1). The shape of the photon pulse is assumed to be Gaussian in all three dimensions and no correlation between spatial position within the pulse and energy spectrum is taken into account. Both of these assumptions are especially unrealistic if the photon beam is produced by backscattering laser photons off the electron beam at IP1. Nevertheless, these simulations have been used extensively to predict pair creation rates at IP2 for the current experimental setup and will still be useful to study new and improved experimental situations.

The development of NI started around June 1994 and a first version simulating nonlinear Compton scattering of electrons in a circularly polarized laser field was running by September of the same year. Since then, the program has been extended and improved continuously. First, the production of electron-positron pairs by high-energy photons via either the multiphoton Breit-Wheeler or the multiphoton trident process was implemented. Then the simulation was extended to include strongfield QED processes in linearly polarized laser fields. Later, the polarization of a Compton-backscattered photon beam and the effect of this polarization on the pair production was implemented, however only for a linearly polarized laser field. Once experimental data became available, a procedure was developed to store results of simulations over wide ranges of possible laser and electron beam parameters in lookup tables. These tables were then interfaced to the analysis software of the experiment and allowed a direct and fast comparison between experimentally measured reaction rates and theoretical predictions for each recorded laser pulse. The current version of the simulation program includes all features necessary to compare the data collected by the E-144 experiment with theory but, of course, is by no means complete.

Also implemented in NI are the interactions between an electron or photon beam with an intense static electromagnetic field. The processes considered are ‘beamstrahlung’ and ’coherent pair production’. However, since we did not study this type of interactions at E-144 (and because time is running out) this part of the program is not documented in this write-up.

The program is written in C and was developed on 486 and Pentium PCs running under DOS. The memory limitations of DOS dictated somewhat the style of the program, *e.g.* many program options are implemented as preprocessor directives and not as run-time parameters, which has the advantage of a smaller (and slightly faster) executable but requires recompiling the code if an option is changed. Later NI was successfully ported to the LINUX and AIX operating systems with the GNU C-compiler. Installing the program on other machines or under other operating systems should be straightforward.

Great care has been taken to make program execution fast. However, since a gain in execution speed usually comes with a price in accuracy of the simulation results, optimizations are implemented either as a selectable program option or as a parameter defining the level of optimization.

2 Basic Formulas

I have no intention to derive the formalism of strongfield QED in this section. However, I believe it is important to list the basic formulas for the many processes exactly in the form they are implemented in NI, including all approximations and units. Most of the formulas are taken from the work of Narozhny, Nikishov and Ritus [1, 2, 3]. In these papers, results are expressed in the form of Lorentz-invariant differential reaction rates (as opposed to cross-sections) which is well suited for numerical calculations. I chose the laboratory (LAB) frame for an explicit evaluation of four-vector scalar products because the center-of-mass (CM) frame is not unique for the collision of an electron or photon beam with a laser pulse, but depends on the number of initial laser photons in the reaction as well as the field intensity (mass shift).

2.1 Symbols and Units

The following list defines some of the symbols used throughout this document:

e, m	charge and mass of electron,
c	speed of light,
p_μ, p'_μ	4-momentum of electron or positron, initial or final state,
E_-, E_+	energy of electron, positron,
γ_-, γ_+	Lorentz factor of electron, positron, *i.e.* $\gamma_\pm = E_\pm/mc^2$,
β_-, β_+	velocity of electron, positron, *i.e.* $\beta_\pm = \sqrt{1 - 1/\gamma_\pm^2}$,
ρ_-, ρ_+	density of electrons, positrons,
$\omega_\mu, \omega, \rho_\omega$	4-momentum, frequency and density of laser photons,
$\omega'_\mu, \omega', \rho_{\omega'}$	4-momentum, frequency and density of high-energy photons,
δ	crossing angle between laser pulse and beam (electron or photon), *e.g.* $\delta = 0$ for a head-on collision,
α	$\alpha = \pi + \delta$, *e.g.* $\alpha = \pi$ for a head-on collision,
θ, φ	polar and azimuthal scattering angle of final state particle, *i.e.* ω' for Compton scattering, positron for pair production,
n	number of initial state laser photons (order of multiphoton process),
η	measure of field strength (see below),
$\bar{m}$	effective mass of electron in field of strength η.

The results in this section are expressed in natural units where $\hbar$ and c are dimensionless and equal to 1 and the unit of energy is GeV. The units and conversion factors for length and time can be derived from the relations $c = 2.998 \times 10^2 \mu\text{m/psec}$ and $\hbar c = 1.97 \times 10^{-10} \text{GeV}\,\mu\text{m}$. In this system, the charge of the electron has the dimensionless value $e = \sqrt{4\pi\alpha} = 0.30282$.

The formulas listed below for the various processes give the differential and total reaction rates of initial particles in the laser field per unit volume and unit time. For example, the expression $dW_n(\omega')/d\omega'$ for nonlinear Compton scattering gives the differential probability per unit volume and per unit time that an electron interacts with n laser photons and emits a single photon with frequency ω'. The number of interactions within given elements of volume (dV), time (dt) and energy ($d\omega'$) is then given by

$$N(dV, dt, d\omega) = \frac{dW_n(\omega')}{d\omega'} \cdot dV \cdot c\, dt \cdot d\omega' \cdot \frac{1}{\hbar c} \,, \tag{1}$$

where the factor of $1/\hbar c$ is required to make the expression dimensionless.

2.2 General Formulas and Relations

2.2.1 Field Strength Parameter η

The dimensionless and invariant parameter η is defined as $\eta \equiv e\sqrt{\langle A_\mu A^\mu \rangle}/mc^2$. In the LAB frame, η can be expressed as (in natural units)

$$\eta = \frac{e\mathcal{E}_{\rm rms}}{m\omega} = \frac{e}{m}\sqrt{\frac{\rho_\omega}{\omega}} \,, \tag{2}$$

where $\mathcal{E}_{\rm rms}$ is the root-mean-square electric field of the laser. With this definition of η, Eq. (2) holds both for a circularly and linearly polarized wave fields. Note however that this definition of η is different from the one used by Nikishov *et al.*. Their η values are bigger by $\sqrt{2}$ for a linearly polarized wave field.

2.2.2 Effective 4-Momentum and Effective Mass

The 4-momentum of a charged particle entering a strong wave field is altered due to continuous absorption and emission of photons. For a particle with 4-momentum p_μ outside the field, the effective 4-momentum $\bar{p}_\mu$ in a field with strength η is given by

$$\bar{p}_\mu = p_\mu + \frac{\eta^2 m^2}{2 p_\mu \omega^\mu}\, \omega_\mu \,, \tag{3}$$

where ω_μ is the 4-momentum of a laser photon. The effective mass $\bar{m}$ of the particle in the field is then obtained by

$$\bar{m}^2 \;\equiv\; \bar{p}_\mu \bar{p}^\mu \;=\; m^2(1+\eta^2). \tag{4}$$

2.2.3 Approximations

The formulas for kinematic variables and relations in the LAB frame can be simplified considerably by the assumption that the beam energy $E_{\rm beam}$ is much bigger than the electron mass. For the experimental conditions of E-144, the ratio is $E_{\rm beam}/mc^2 \sim 10^5$. This assumption about $E_{\rm beam}$ can be translated into the two basic approximations

$$\begin{aligned} \theta \;&\sim\; 1/\gamma \ll 1 \qquad \text{and} \\ \eta \;&\ll\; \gamma \,, \end{aligned} \tag{5}$$

where $\gamma = E/mc^2$ with E the energy of the particle interacting with the laser field. The two approximations in Eq. (5) have been used to derive the form of the formulas implemented in NI.

2.2.4 Bessel Functions

The expression for the differential reaction rate of a nonlinear QED process of order n in a circularly polarized wave includes the Bessel functions $J_{n-1}(z)$, $J_n(z)$ and $J_{n+1}(z)$. The two lowest order Bessel functions $J_0(z)$ and $J_1(z)$ can be expressed by asymptotic series and all higher orders are then derived by the recurrence formula

$$J_{n+1}(z) = \frac{2n}{z} J_n(z) - J_{n-1}(z). \tag{6}$$

This procedure is implemented in NI with the help of three routines from *'Numerical Recipes in C'*, *i.e.* `bessj(), bessj0(), bessj1()`.

2.2.5 A_i Functions

For a linearly polarized wave, differential reaction rates are expressed by the real functions $A_0(n,a,b)$, $A_1(n,a,b)$ and $A_2(n,a,b)$, defined as

$$A_i(n,a,b) \equiv \frac{1}{\pi} \int_0^\pi d\nu \ \cos^i \nu \cdot \cos[(a + 2b\cos\nu)\sin\nu - n\nu] \ , \ i = 0,1,2 \ . \tag{7}$$

The functions $A_1(n,a,b)$ and $A_2(n,a,b)$ can be expressed by lower and higher orders n of A_0 as

$$A_1(n,a,b) \ = \ \frac{1}{2} \left[A_0(n-1,a,b) + A_0(n+1,a,b) \right], \tag{8}$$

$$A_2(n,a,b) \ = \ \frac{1}{4} \left[A_0(n-2,a,b) + 2A_0(n,a,b) + A_0(n+2,a,b) \right]. \tag{9}$$

The symmetry of $A_i(n,a,b)$, $i = 0,1,2$, with respect to a is given by

$$A_i(n,-a,b) = (-1)^{n+i} A_i(n,a,b). \tag{10}$$

In addition, the following important relation holds for the three functions evaluated at the same parameter values n, a and b:

$$(n + 2b)A_0 \ - \ aA_1 \ - \ 4bA_2 \ = \ 0. \tag{11}$$

In principle, a numeric integration (*i.e.* sumation) of the A_i-functions according to Eq. (7) is straightforward. However, if $a = b = 0$ the integrand reduces to $\cos^i \nu \ \cos(n\nu)$ and the integral evaluates to zero for many combinations of n and i. For these combinations of n and i and small values of a and b the value of $A_i(n,a,b)$ evaluated by summation can become dominated by numerical inaccuracies. This problem can be solved by expanding the term

$\cos[(a+2b\cos\nu)\sin\nu - n\nu]$ in a power series and solving the integrals analytically for the leading terms in the series.

Both Glenn and Kostya came up with a solution in which the integrand of $A_0(n,a,b)$ is expressed as a power series of η. This approach is motivated by the fact that $a \propto \eta$ and $b \propto \eta^2$ and therefore $b \ll a \ll 1$ for $\eta \ll 1$. Solving the integrals for the leading terms in the series results in

$$\begin{aligned} A_0(n,a,b) &= \sum_{j=0}^{n/2} \frac{a^{n-2j}\, b^j}{(n-2j)!\, j!} \cdot \left(\frac{1}{2}\right)^{n-j} \qquad \text{for } n \geq 0 \quad \text{and} \\ A_0(-1,a,b) &= -\frac{a}{2}\,, \end{aligned} \tag{12}$$

where the convention is used that $n/2 \equiv (n-1)/2$ for an odd value of n. The values for $A_1(n,a,b)$ and $A_2(n,a,b)$ for $n \geq 1$ are then easily obtained with relations (8) and (9).

However, a is also proportional to $\cos\phi$ (see below) and therefore the relation $b \ll a$ does not always apply, even for $\eta \ll 1$. I tried a more symmetric approach in a and b by using the substitution $\epsilon = (a+2b\cos\nu)\sin\nu$ and expanding the integrand of $A_0(n,a,b)$ in a power series of ϵ. The result of this procedure is

$$\begin{aligned} A_0(n,a,b) &= -\frac{\bar{a}\,\bar{b}^{\frac{n}{2}+2}}{\left(\frac{n}{2}+1\right)!} - \frac{\bar{a}\,\bar{b}^{\frac{n}{2}+1}}{\left(\frac{n}{2}+1\right)!} + \frac{\bar{a}\,\bar{b}^{\frac{n}{2}}}{\left(\frac{n}{2}\right)!} - \frac{\bar{a}^3\,\bar{b}^{\frac{n}{2}}}{2\left(\frac{n}{2}\right)!} \\ &\quad + \frac{\bar{a}^3\,\bar{b}^{\frac{n}{2}-1}}{6\left(\frac{n}{2}-1\right)!} + \frac{\bar{a}^5\,\bar{b}^{\frac{n}{2}-2}}{120\left(\frac{n}{2}-2\right)!} \qquad n > 0,\ \text{odd} \\ A_0(-1,a,b) &= \bar{a}\,\bar{b}^2 - \bar{a}\,\bar{b} - \bar{a} + \frac{1}{2}\bar{a}^3 \qquad n = -1 \\ A_0(n,a,b) &= -\frac{\bar{b}^{\frac{n}{2}+2}}{\left(\frac{n}{2}+1\right)!} + \frac{\bar{b}^{\frac{n}{2}}}{\left(\frac{n}{2}\right)!} - \frac{\bar{a}^2\bar{b}^{\frac{n}{2}}}{\left(\frac{n}{2}\right)!} + \frac{\bar{a}^2\bar{b}^{\frac{n}{2}-1}}{2\left(\frac{n}{2}-1\right)!} \\ &\quad + \frac{\bar{a}^4\bar{b}^{\frac{n}{2}-2}}{24\left(\frac{n}{2}-2\right)!} \qquad n \geq 0,\ \text{even} \end{aligned} \tag{13}$$

with $\bar{a} = a/2$ and $\bar{b} = b/2$ and where again the convention is used that $n/2 \equiv (n-1)/2$ for an odd value of n. In addition, it is implied that only terms are considered where the exponent of b is positive or equal to zero, *e.g.* for n odd the 5^{th} term is used only if $n \geq 3$ and the last term if $n \geq 5$.

None of the three methods explained above (*i.e.* numeric integration, Eq. (12) and Eq. (13)) is by itself sufficient to calculate the $A_i(n,a,b)$ functions reliably for all combinations of parameters. To determine how successful a method is for a given parameter set, I used relation (11) to defined the following (maybe somewhat redundant) measures of inaccuracy:

$$\Delta A(n,a,b) \equiv \frac{|(n+2b)A_0 - aA_1 - 4bA_2|}{|(n+2b)A_0| + |aA_1| + |4bA_2|}\,,$$

$$\begin{aligned}
\Delta A_0(n,a,b) &\equiv \frac{\left|A_0 - \frac{aA_1+4bA_2}{(n+2b)}\right|}{|A_0| + \left|\frac{aA_1+4bA_2}{(n+2b)}\right|}, \\
\Delta A_1(n,a,b) &\equiv \frac{\left|A_1 - \frac{(n+2b)A_0-4bA_2}{a}\right|}{|A_1| + \left|\frac{(n+2b)A_0-4bA_2}{a}\right|}, \\
\Delta A_2(n,a,b) &\equiv \frac{\left|A_2 - \frac{(n+2b)A_0-aA_1}{4b}\right|}{|A_2| + \left|\frac{(n+2b)A_0-aA_1}{4b}\right|}.
\end{aligned} \tag{14}$$

The algorithm implemented in NI to evaluate the functions $A_i(n,a,b)$ relies in principle on all three methods mentioned above. However, the series defined in Eq. (12) is used only if $|a/b| > 0.3$. Similarly, for the series of Eq. (13) to be used, the relation $|a|+|b| < 0.3$ must hold. If more than one method is used, the program uses the values that give the smallest errors as defined in (14)

2.3 Nonlinear Compton Scattering

By nonlinear Compton scattering (NLCS) we refer to the coherent absorption of several wave photons and emission of a single (higher energy) photon by an electron or positron, *i.e.*

$$e + n\omega \quad \rightarrow \quad e' + \omega' . \tag{15}$$

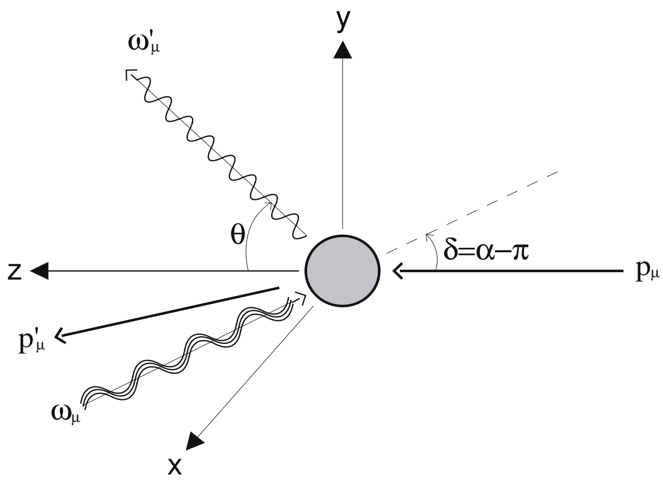

Figure 1: Kinematic variables in the LAB frame for the nonlinear Compton scattering process.

The kinematic variables in the LAB frame for NLCS are shown in Fig. 1. The momentum 4-vectors of the initial and final states are:

$$\omega_\mu \;=\; (\omega,\vec{k}) \;=\; \omega\,(1,\sin\alpha,0,\cos\alpha)\;, \tag{16}$$

$$p_\mu = (E_\pm, \vec{p}_\pm) = E_\pm\ (1, 0, 0, \beta_\pm)\ , \tag{17}$$
$$\omega'_\mu = (\omega', \vec{k}') = \omega'\ (1, \sin\theta\cos\varphi, \sin\theta\sin\varphi, \cos\theta), \tag{18}$$

where φ is the azimuthal angle of the emitted photon ω' and is not shown in Fig. 1. We define the following invariants and express their values by kinematic variables in the LAB system:

$$u \equiv \frac{\omega_\mu \omega'^\mu}{\omega_\mu \bar{p}'^\mu} \simeq \frac{\omega'}{E_\pm - \omega'}\ , \tag{19}$$
$$u_1 \equiv \frac{2\omega_\mu \bar{p}^\mu}{m^2(1+\eta^2)} \simeq \frac{2E_\pm \omega(1-\cos\alpha)}{m^2(1+\eta^2)}\ , \tag{20}$$
$$u_n \equiv n \cdot u_1\ . \tag{21}$$

The relation between the scattering angle θ and the energy ω' of the emitted photon is

$$\omega'(n,\theta) \simeq E_\pm \cdot \frac{nu_1(1+\eta^2)}{(nu_1+1)(1+\eta^2) + \gamma_\pm^2\ \theta^2}\ . \tag{22}$$

The energy spectrum of the scattered photon is within $[0, \omega'_{\max}(n)]$ and the upper limit occurs for $\theta \simeq 0$ and is given by

$$\omega'_{\max}(n)\ \simeq\ E_\pm \cdot \frac{nu_1(1+\eta^2)}{(nu_1+1)(1+\eta^2)}\ =\ \frac{2nE_\pm^2\omega(1-\cos\alpha)}{m^2(1+\eta^2) + 2nE_\pm\omega(1-\cos\alpha)}\ . \tag{23}$$

2.3.1 Circularly Polarized Field

The differential reaction rate for nonlinear Compton scattering in a circularly polarized wave is given by [2]

$$\frac{dW_n(\omega')}{d\omega'} = \frac{e^2 m^2 \rho_\pm}{16\pi E_\pm^2} \left\{ -4J_n^2(z) + \eta^2 \left(2 + \frac{u^2}{1+u}\right) \left(J_{n-1}^2(z) + J_{n+1}^2(z) - 2J_n^2(z)\right) \right\} \tag{24}$$

where

$$z = \frac{2\eta}{u_1} \sqrt{\frac{u(nu_1 - u)}{1+\eta^2}}\ . \tag{25}$$

The total reaction rates for Compton scattering of order $n = 1$ and $n = 2$ in a circularly polarized wave with intensity parameter $\eta^2 \ll 1$ can be approximated (up to terms in η^4) by [2]

$$W_1 = \frac{e^2 m^2 \rho_\pm}{16\pi E_\pm}\ \eta^2 \left\{ \left(1 - \frac{4}{u_1} - \frac{8}{u_1^2}\right) \ln(1+u_1) + \frac{1}{2} + \frac{8}{u_1} - \frac{1}{2(1+u_1)^2} - \right.$$
$$\eta^2 \left[2 + \frac{44}{3u_1} - \frac{16}{u_1^2} - \frac{16}{u_1^3} - \frac{2}{1+u_1} - \right.$$

$$\left(\frac{8}{u_1} + \frac{8}{u_1^2} - \frac{24}{u_1^3} - \frac{16}{u_1^4}\right) \ln(1+u_1)\Big]\Big\} \ , \tag{26}$$

$$\begin{aligned} W_2 &= \frac{e^2 m^2 \rho_\pm}{16\pi E_\pm}\, \eta^4 \left\{ 2 + \frac{8}{3u_2} - \frac{64}{u_2^2} - \frac{64}{u_2^3} - \frac{2}{1+u_2} - \right. \\ &\left. \left(\frac{4}{u_2} - \frac{24}{u_2^2} - \frac{96}{u_2^3} - \frac{64}{u_2^4}\right) \ln(1+u_2) \right\} \ . \end{aligned} \tag{27}$$

2.3.2 Linearly Polarized Field

The differential reaction rate for nonlinear Compton scattering in a linearly polarized wave is given by [1]

$$\frac{dW_n(\omega')}{d\omega'} = \frac{e^2 m^2 \rho_\pm}{2\pi^2 E_\pm^2} \int_0^{\pi/2} d\phi \left\{ -A_0^2 + \eta^2 \left(2 + \frac{u^2}{1+u}\right) \left(A_1^2 - A_0\, A_2\right) \right\} \tag{28}$$

where $A_i \equiv A_i(n,a,b)$. The functions $A_i(n,a,b)$ are described in section 2.2.5 and the parameters a and b are defined as

$$\begin{aligned} a &\equiv \sqrt{2} m\eta \left(\frac{\varepsilon_\mu p^\mu}{\omega_\mu p^\mu} - \frac{\varepsilon_\mu p'^\mu}{\omega_\mu p'^\mu}\right) \simeq \frac{\sqrt{8} Q\ n\eta}{1+\eta^2+Q^2} \cdot \cos\phi \ , \end{aligned} \tag{29}$$

$$\begin{aligned} b &\equiv 4m^2\eta^2 \left(\frac{1}{\omega_\mu p^\mu} - \frac{1}{\omega_\mu p'^\mu}\right) \simeq \frac{-(n/2)\eta^2}{1+\eta^2+Q^2}, \end{aligned} \tag{30}$$

where $\varepsilon_\mu = (\varepsilon_0, \vec{\varepsilon})$ is the polarization 4-vector of the laser photons, ϕ is the angle between the planes $(\vec{k}, \vec{p}')$ and $(\vec{k}, \vec{\varepsilon})$ in the CM frame and Q is defined by

$$Q^2 = (1+\eta^2)\left(\frac{n u_1}{u} - 1\right) . \tag{31}$$

Note that b is defined with opposite sign compared to the definition in [1]. However, in this document the sign is also reversed in the definition of the functions $A_i(n,a,b)$ and other relations in section 2.2.5.

The total reaction rates for Compton scattering of order $n=1$ and $n=2$ in a linearly polarized wave with intensity parameter $\eta^2 \ll 1$ can be approximated (up to terms in η^4) by [3]

$$\begin{aligned} W_1 &= \frac{e^2 m^2 \rho_\pm}{16\pi E_\pm}\, \eta^2 \left\{ \left(1 - \frac{4}{u_1} - \frac{8}{u_1^2}\right) \ln(1+u_1) + \frac{1}{2} + \frac{8}{u_1} - \frac{1}{2(1+u_1)^2} - \right. \\ &\frac{\eta^2}{2} \left[3 + \frac{22}{u_1} - \frac{36}{u_1^2} - \frac{48}{u_1^3} - \frac{3}{2(1+u_1)} - \frac{1}{2(1+u_1)^2} - \right. \\ &\left. \left. \left(\frac{13}{u_1} + \frac{8}{u_1^2} - \frac{60}{u_1^3} - \frac{48}{u_1^4}\right) \ln(1+u_1) \right] \right\} \ , \end{aligned} \tag{32}$$

$$
\begin{aligned}
W_2 \;=\; & \frac{e^2 m^2 \rho_\pm}{16\pi E_\pm}\,\frac{\eta^4}{2}\left\{3-\frac{4}{u_2}-\frac{144}{u_2^2}-\frac{192}{u_2^3}+\frac{1}{2(1+u_2)}-\frac{1}{2(1+u_2)^2}-\right.\\
& \left.\left(\frac{5}{u_2}-\frac{60}{u_2^2}-\frac{240}{u_2^3}-\frac{192}{u_2^4}\right)\ln(1+u_2)\right\}\;. \qquad (33)
\end{aligned}
$$

The polarization of the emitted photon ω' becomes important if further interactions with the wave field, *e.g.* Breit-Wheeler pair production, are considered. The differential reaction rates for final state photons ω' with a polarization either parallel ($\|$) or perpendicular ($\perp$) to the polarization of the wave photons ω are [5]:

$$
\frac{dW_n^{\|}(\omega')}{d\omega'} = \frac{e^2 m^2 \rho_\pm}{2\pi^2 E_\pm^2}\int_0^{\pi/2} d\phi\left\{-2\eta^2\sigma' A_0^2+\eta^2\left(2+\frac{u^2}{2(1+u)}\right)\left(A_1^2-A_0\,A_2\right)\right\}\;, \quad (34)
$$

$$
\frac{dW_n^{\perp}(\omega')}{d\omega'} = \frac{e^2 m^2 \rho_\pm}{2\pi^2 E_\pm^2}\int_0^{\pi/2} d\phi\left\{-(1-2\eta^2\sigma')A_0^2+\eta^2\frac{u^2}{2(1+u)}\left(A_1^2-A_0\,A_2\right)\right\}\;, \quad (35)
$$

where

$$
\sigma' \equiv -\left[\frac{1}{2}+\frac{n}{4\beta}+\left(\frac{\alpha}{8\beta}\right)^2\right]\;. \quad (36)
$$

The polarization state of the backscattered photons can be summarized by the spectrum $P(\omega')$ which gives the fraction of photons at energy ω' with a polarization parallel to the wave, *i.e.*

$$
P(\omega') \equiv \frac{\sum_n\left(dW_n^{\|}(\omega')/d\omega'\right)}{\sum_n\left(dW_n^{\|}(\omega')/d\omega'\right)\;+\;\left(dW_n^{\perp}(\omega')/d\omega'\right)} = \frac{\sum_n\left(dW_n^{\|}(\omega')/d\omega'\right)}{\sum_n\left(dW_n(\omega')/d\omega'\right)}\;. \quad (37)
$$

2.4 Multiphoton Breit-Wheeler Pair Production

With the multiphoton Breit-Wheeler (MPBW) process we refer to the e^+e^- pair production by the coherent interaction of a high energy photon and several wave photons, *i.e.*

$$
\omega' \;+\; n\omega \quad\rightarrow\quad e^+\,e^-\;. \quad (38)
$$

The kinematic variables in the LAB frame for the MPBW process are shown in Fig. 2. The momentum 4-vectors of the initial and final states are:

$$
\begin{aligned}
\omega_\mu &= (\omega,\vec{k}) \;=\; \omega\,(1,\sin\alpha,0,\cos\alpha)\;, & (39)\\
\omega'_\mu &= (\omega',\vec{k'}) \;=\; \omega'\,(1,0,0,1)\;, & (40)\\
p_\mu &= (E_\pm,\vec{p}_\pm) \;=\; E_\pm\,(1,\beta_\pm\sin\theta\cos\varphi,\beta_\pm\sin\theta\sin\varphi,\beta_\pm\cos\theta), & (41)
\end{aligned}
$$

where φ is the azimuthal angle of the created positron (or electron) and is not shown in Fig. 2. We define the following invariants and express their values by kinematic variables in

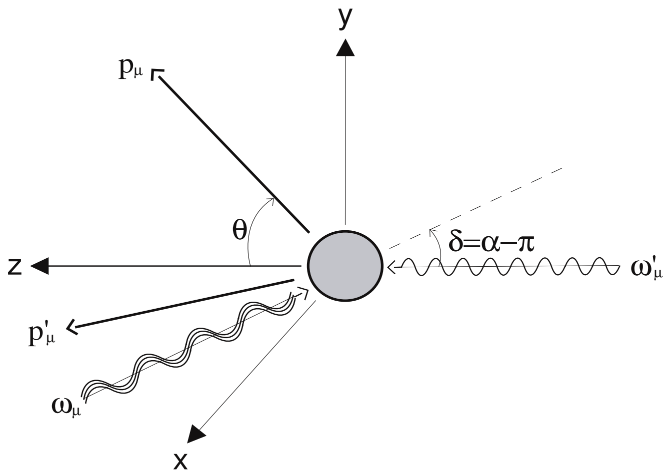

Figure 2: Kinematic variables in the LAB frame for the multiphoton Breit-Wheeler process.

the LAB system:

$$u \equiv \frac{(\omega_\mu \omega'^\mu)^2}{4(\omega_\mu \bar{p}^\mu)(\omega_\mu \bar{p}'^\mu)} \simeq \frac{\omega'^2}{4E_\pm(\omega' - E_\pm)} , \quad (42)$$

$$u_1 \equiv \frac{\omega_\mu \omega'^\mu}{2m^2(1+\eta^2)} \simeq \frac{\omega\omega'(1-\cos\alpha)}{2m^2(1+\eta^2)} , \quad (43)$$

$$u_n \equiv n \cdot u_1 . \quad (44)$$

The number of wave photons kinematically required to produce a e^+e^- pair is given by the integer bigger or equal to the real number

$$n_0 \equiv \frac{1}{u_1} \simeq \frac{2m^2(1+\eta^2)}{\omega\omega'(1-\cos\alpha)} . \quad (45)$$

With relation (45) we obtain the minimum photon energy $\omega'_{\rm min}$ required to produce a pair with n wave photons:

$$\omega'_{\rm min} = \frac{2m^2(1+\eta^2)}{n\omega(1-\cos\alpha)}. \quad (46)$$

The energy spectrum of the produced electrons and positrons is within $[E_{\rm min}, E_{\rm max}]$ given by

$$E_{\substack{\rm max \\ \rm min}} = \frac{\omega'}{2}\left(1 \pm \sqrt{n_0/n}\right) = \frac{\omega'}{2}\left(1 \pm \sqrt{1 - \frac{2m^2(1+\eta^2)}{n\omega\omega'(1-\cos\alpha)}}\right) . \quad (47)$$

2.4.1 Circularly Polarized Field

The differential reaction rate for the multiphoton Breit-Wheeler process in a circularly polarized wave is given by [2]

$$\frac{dW_n(E_\pm)}{dE_\pm} = \frac{e^2 m^2 \rho_{\omega'}}{8\pi\omega'^2}\left\{2J_n^2(z) + \eta^2\,(2u-1)\left(J_{n-1}^2(z) + J_{n+1}^2(z) - 2J_n^2(z)\right)\right\} \quad (48)$$

for $n \geq n_0$ and with

$$z = \frac{2\eta}{u_1}\sqrt{\frac{u(nu_1 - u)}{1+\eta^2}} \,. \tag{49}$$

The total reaction rates for MPBW pair production of order $n = 1$ and $n = 2$ in a circularly polarized wave with intensity parameter $\eta^2 \ll 1$ can be approximated (up to terms in η^4) by [2]

$$\begin{aligned} W_1 &= \frac{e^2 m^2 \rho_{\omega'}}{16\pi\omega'}\,\eta^2 \left\{ 2\left[\left(2 + \frac{2}{u_1} - \frac{1}{u_1^2}\right)\tanh^{-1}\sqrt{1-\frac{1}{u_1}} - \sqrt{1-\frac{1}{u_1}}\left(1+\frac{1}{u_1}\right)\right] - \right. \\ &\quad \eta^2\left[\sqrt{1-\frac{1}{u_1}}\left(4 - \frac{10}{3u_1} - \frac{13}{6u_1^2} + \frac{5}{4u_1^3}\right) + \right. \\ &\quad \left.\left.\left(\frac{4}{u_1} - \frac{2}{u_1^2} - \frac{3}{u_1^3} + \frac{5}{4u_1^4}\right)\tanh^{-1}\sqrt{1-\frac{1}{u_1}}\right]\right\} \,, \end{aligned} \tag{50}$$

$$\begin{aligned} W_2 &= \frac{e^2 m^2 \rho_{\omega'}}{16\pi\omega'}\,\eta^4 \left\{ \sqrt{1-\frac{1}{u_2}}\left(4 + \frac{2}{3u_2} - \frac{26}{3u_2^2} + \frac{5}{u_2^3}\right) + \right. \\ &\quad \left.\left(\frac{6}{u_2^2} - \frac{12}{u_2^3} + \frac{5}{u_2^4}\right)\tanh^{-1}\sqrt{1-\frac{1}{u_2}}\right\} \,. \end{aligned} \tag{51}$$

2.4.2 Linearly Polarized Field

The differential reaction rate for the multiphoton Breit-Wheeler process with unpolarized photons in a linearly polarized wave is given by [1]

$$\frac{dW_n(E_\pm)}{dE_\pm} = \frac{e^2 m^2 \rho_{\omega'}}{2\pi^2\omega'^2}\int_0^{\pi/2} d\phi \left\{A_0^2 + 2\eta^2\,(2u-1)\left(A_1^2 - A_0\,A_2\right)\right\} \tag{52}$$

for $n \geq n_0$ and with $A_i \equiv A_i(n,a,b)$. The functions $A_i(n,a,b)$ are described in section 2.2.5 and the parameters a and b are defined as

$$\begin{aligned} a &\equiv \sqrt{2}m\eta\left(\frac{\varepsilon_\mu p^\mu}{\omega_\mu p^\mu} - \frac{\varepsilon_\mu p'^\mu}{\omega_\mu p'^\mu}\right) \simeq \frac{\sqrt{2}m\eta\omega'\theta}{\omega(\omega' - E_\pm)(1-\cos\alpha)} \cdot \cos\phi \,, \end{aligned} \tag{53}$$

$$\begin{aligned} b &\equiv 4m^2\eta^2\left(\frac{1}{\omega_\mu p^\mu} - \frac{1}{\omega_\mu p'^\mu}\right) \simeq \frac{m^2\eta^2(\omega' - 2E_\pm)}{4E_\pm\omega(\omega' - E_\pm)(1-\cos\alpha)}, \end{aligned} \tag{54}$$

where $\varepsilon_\mu = (\varepsilon_0, \vec{\varepsilon})$ is the polarization 4-vector of the laser photons, ϕ is the angle between the planes $(\vec{k}, \vec{p}')$ and $(\vec{k}, \vec{\varepsilon})$ in the CM frame and the scattering angle θ is given by

$$\theta^2 = 2n\omega(1-\cos\alpha)\left(\frac{1}{E_\pm} - \frac{1}{\omega'}\right) - \frac{m^2(1+\eta^2)}{E_\pm^2} \,. \tag{55}$$

Note that b is defined with opposite sign compared to the definition in [1]. However, in this document the sign is also reversed in the definition of the functions $A_i(n,a,b)$ and other relations in section 2.2.5.

The total reaction rates for MPBW pair creation of order $n = 1$ and $n = 2$ in a linearly polarized wave with intensity parameter $\eta^2 \ll 1$ can be approximated (up to terms in η^4) by [3]

$$\begin{aligned}
W_1 &= \frac{e^2 m^2 \rho_{\omega'}}{16\pi\omega'}\,\eta^2 \left\{ 2\left[\left(2+\frac{2}{u_1}-\frac{1}{u_1^2}\right)\tanh^{-1}\sqrt{1-\frac{1}{u_1}} - \sqrt{1-\frac{1}{u_1}}\left(1+\frac{1}{u_1}\right)\right] - \right. \\
&\qquad \frac{\eta^2}{2}\left[\sqrt{1-\frac{1}{u_1}}\left(6-\frac{5}{u_1}-\frac{5}{u_1^2}+\frac{15}{4u_1^3}\right) + \right. \\
&\qquad \left.\left.\left(\frac{8}{u_1}-\frac{2}{u_1^2}-\frac{15}{2u_1^3}+\frac{15}{4u_1^4}\right)\tanh^{-1}\sqrt{1-\frac{1}{u_1}}\right]\right\}, \qquad (56) \\
W_2 &= \frac{e^2 m^2 \rho_{\omega'}}{16\pi\omega'}\,\frac{\eta^4}{2}\left\{\sqrt{1-\frac{1}{u_2}}\left(6+\frac{3}{u_2}-\frac{20}{u_2^2}+\frac{15}{u_2^3}\right) + \right. \\
&\qquad \left. 15\left(\frac{1}{u_2^2}-\frac{2}{u_2^3}+\frac{1}{u_2^4}\right)\tanh^{-1}\sqrt{1-\frac{1}{u_2}}\right\}. \qquad (57)
\end{aligned}$$

The pair production rate depends on the polarization of the photons interacting with the wave and the expression in Eq. (52) is valid only for an unpolarized photon beam. If the polarization state of the photon beam is described by the spectrum $P(\omega')$ as defined in Eq. (37), *i.e.* the fraction of photons at energy ω' with a polarization parallel to the wave, the differential reaction rate for the MPBW process is given by [1]:

$$\frac{dW_n^P(E_\pm)}{dE_\pm} = \frac{e^2 m^2 \rho_{\omega'}}{2\pi^2\omega'^2}\cdot 2\cdot\int_0^{\pi/2} d\phi \left\{(1-P)A_0^2 + 2\eta^2(2P-1)\sigma' A_0^2 + 2\eta^2(u-P)\left(A_1^2 - A_0\,A_2\right)\right\}, \qquad (58)$$

where $P \equiv P(\omega')$ and σ' are defined in Eqs. (36) and (37). The formulas for the two special cases of a parallel ($\|$) polarized ($P = 1$) and a perpendicular ($\perp$) polarized ($P = 0$) photon beam are then:

$$\frac{dW_n^{\|}(E_\pm)}{dE_\pm} = \frac{e^2 m^2 \rho_{\omega'}}{2\pi^2\omega'^2}\cdot 2\cdot\int_0^{\pi/2} d\phi \left\{2\eta^2\sigma' A_0^2 + 2\eta^2(u-1)\left(A_1^2 - A_0\,A_2\right)\right\}, \qquad (59)$$

$$\frac{dW_n^{\perp}(E_\pm)}{dE_\pm} = \frac{e^2 m^2 \rho_{\omega'}}{2\pi^2\omega'^2}\cdot 2\cdot\int_0^{\pi/2} d\phi \left\{(1-2\eta^2\sigma')A_0^2 + 2\eta^2 u\left(A_1^2 - A_0\,A_2\right)\right\}, \qquad (60)$$

2.5 Klein-Nishina Approximation

The Klein-Nishina formula for Compton scattering (KNCS) is an approximate expression for Compton scattering in weak fields, *i.e.* only the linear ($n = 1$) process is considered and the mass shift effect ($\bar{m}^2 = m^2(1+\eta^2)$) is neglected.

The kinematic variables are defined as in Fig. 1 for NLCS and the differential reaction rate is

$$\frac{dW(\omega')}{d\omega'} = \frac{e^2 m^2 \rho_\pm}{16\pi E_\pm^2}\,\eta^2\left\{2+\frac{u^2}{1+u}-\frac{4u}{u_1}\left(1-\frac{u}{u_1}\right)\right\}, \qquad (61)$$

where u and u_1 are defined as in Eq. (19) and (20), except that the effective 4-momentum $\bar{p}'_\mu$ is replaced by p'_μ:

$$u \equiv \frac{\omega_\mu \omega'^\mu}{\omega_\mu p'^\mu} \simeq \frac{\omega'}{E_\pm - \omega'} , \tag{62}$$

$$u_1 \equiv \frac{2\omega_\mu p^\mu}{m^2} \simeq \frac{2E_\pm \omega(1-\cos\alpha)}{m^2} . \tag{63}$$

The expressions for the scattered photon energy $\omega'(\theta)$ and the upper limit $\omega'_{\max}$ are (compare to Eq. (22) and (23)):

$$\omega'(\theta) \simeq E_\pm \cdot \frac{u_1}{(1+u_1)+\gamma_\pm^2\,\theta^2} , \tag{64}$$

$$\omega'_{\max} \simeq E_\pm \cdot \frac{u_1}{1+u_1} = \frac{2E_\pm^2\omega(1-\cos\alpha)}{m^2+2E_\pm\omega(1-\cos\alpha)} , \tag{65}$$

and the total reaction rate for KNCS is given by (compare to Eq. (26) and (32))

$$W = \frac{e^2 m^2 \rho_\pm}{16\pi E_\pm}\,\eta^2 \left\{ \left(1-\frac{4}{u_1}-\frac{8}{u_1^2}\right)\ln(1+u_1)+\frac{1}{2}+\frac{8}{u_1}-\frac{1}{2(1+u_1)^2}\right] . \tag{66}$$

2.6 Multiphoton Trident Pair Production

With the multiphoton trident process we refer to the e^+e^- pair production by the coherent interaction of a virtual photon from the field of a charged particle with several wave photons, *i.e.*

$$e + n\omega \rightarrow e'\, e^+e^- . \tag{67}$$

A complete theory of reaction (67) in a strong field does not exist at present. Therefore, we based our calculation of this process on a two-step model in which the beam electron emits a virtual photon according to the Weizsaсker-Williams approximation and the virtual photon combines with the wave photons to produce a e^+e^- pair according to the theory of the multiphoton Breit-Wheeler (MPBW) process, *i.e.*

$$e \rightarrow e' + \omega' , \tag{68}$$

$$\omega' + n\omega \rightarrow e^+e^- . \tag{69}$$

I will refer to this two-step model as the WWBW process and a detailed description can be found in Ref. [6]. The kinematic variables in the LAB frame for the WWBW process are shown in Fig. 3. The momentum 4-vectors in the reaction are:

$$\omega_\mu = (\omega, \vec{k}) \quad \text{wave photon,} \tag{70}$$

$$p_\mu = (E, \vec{p}) \quad \text{charged particle initial state,} \tag{71}$$

$$p'_\mu = (E', \vec{p}') \quad \text{charged particle final state,} \tag{72}$$

$$p_{\pm_\mu} = (E_\pm, \vec{p}_\pm) \quad e^+ \text{ and } e^- \text{ from pair creation,} \tag{73}$$

$$\omega'_\mu = (\omega', \vec{k}') \quad \text{intermediate virtual photon.} \tag{74}$$

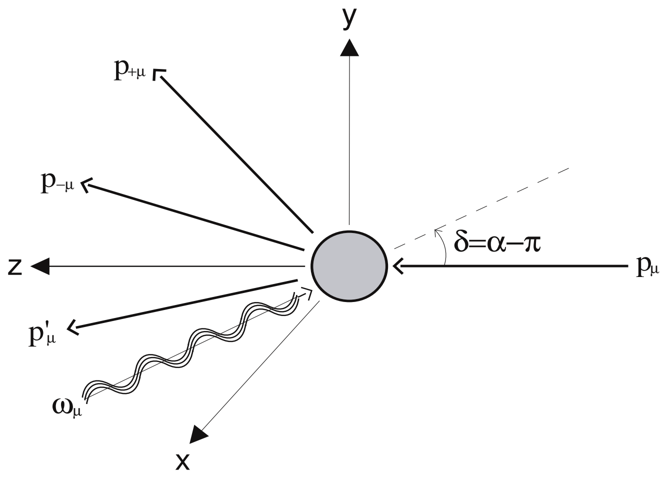

Figure 3: Kinematic variables in the LAB frame for the multiphoton trident process.

The square of the center-of-mass energy in the multiphoton trident process (s) and its minimum value ($s_{\min}$) are given by

$$s \equiv (\bar{p}_\mu + n\omega_\mu)^2 = (\bar{p}'_\mu + \bar{p}_{+\mu} + \bar{p}_{-\mu})^2 = m^2(1+\eta^2) + 2nE\omega(1-\cos\alpha) , \tag{75}$$
$$s_{\min} = (3\bar{m})^2 = 9m^2 (1+\eta^2). \tag{76}$$

From these two relations, it follows that the minimum number of wave photons kinematically required to produce a pair is (compare to Eq. (45))

$$n_0 = \frac{4m^2(1+\eta^2)}{E\omega(1-\cos\alpha)} . \tag{77}$$

For reaction (69), *i.e.* the second step in the WWBW process, the square of the center-of-mass energy (s') and its extreme values ($s'_{\min}, s'_{\max}$) are

$$s' \equiv (\omega'_\mu + n\omega_\mu)^2 = (\bar{p}_{+\mu} + \bar{p}_{-\mu})^2 = 2n\omega\omega'(1-\cos\alpha) , \tag{78}$$
$$s'_{\min} = 4m^2(1+\eta^2) , \tag{79}$$
$$s'_{\max} = \left(\sqrt{s} - m\sqrt{1+\eta^2}\right)^2 . \tag{80}$$

Note that Eq. (80) relates the kinematics of reaction (69) with the center-of-mass energy of the trident process (67) and provides an effective upper limit for the energy of the intermediate virtual photon, which can be substantially lower than the charged particle energy E. With this two-step model, the differential reaction rate for the multiphoton trident process is

$$\frac{dW^{(\mathrm{WWBW})}(E_\pm)}{dE_\pm} = \frac{2\alpha}{\pi} \sum_{n\geq n_0} \int_{s'_{\min}}^{s'_{\max}} \frac{ds'}{s'} \ln\left(\frac{s'_{\max}}{s'}\right) \cdot \frac{dW_n^{(\mathrm{MPBW})}(E_\pm)}{dE_\pm} , \tag{81}$$

where $\alpha = e^2/\hbar c$ is the fine structure constant. For convenience we want to replace the integration over s' in Eq. (81) by an integration over ω'. Using relations (78) one finds

$$
\begin{aligned}
ds'/s' &= d\omega'/\omega' \,, && (82)\\
s'_{\max}/s' &= \omega'_{\max}/\omega' \,, && (83)\\
\omega'_{\max} &\equiv \frac{s'_{\max}}{2n\omega(1-\cos\alpha)} = \frac{\left[\sqrt{m^2(1+\eta^2)+2En\omega(1-\cos\alpha)} - m\sqrt{1+\eta^2}\right]^2}{2n\omega(1-\cos\alpha)} \,, && (84)\\
\omega'_{\min} &\equiv \frac{s'_{\min}}{2n\omega(1-\cos\alpha)} = \frac{2m^2(1+\eta^2)}{n\omega(1-\cos\alpha)} \,, && (85)
\end{aligned}
$$

and therefore

$$\frac{dW^{(\mathrm{WWBW})}(E_\pm)}{dE_\pm} = \frac{2\alpha}{\pi} \sum_{n\geq n_0} \int_{\omega'_{\min}}^{\omega'_{\max}} \frac{d\omega'}{\omega'} \ln\left(\frac{\omega'_{\max}}{\omega'}\right) \cdot \frac{dW_n^{(\mathrm{MPBW})}(E_\pm)}{dE_\pm} \,. \quad (86)$$

3 Modeling Beam and Laser Pulses

In order to calculate the reaction rates discussed in the previous section for a given point in space and time, the density of beam particles ρ_{beam} and laser photons ρ_ω at this space-time point (STP) needs to be known. These densities are modeled as three-dimensional Gaussian distributions, cylindrical for the beam and focused for the laser pulse. Each pulse is described in its own coordinate system (CS), as shown in Fig 4.

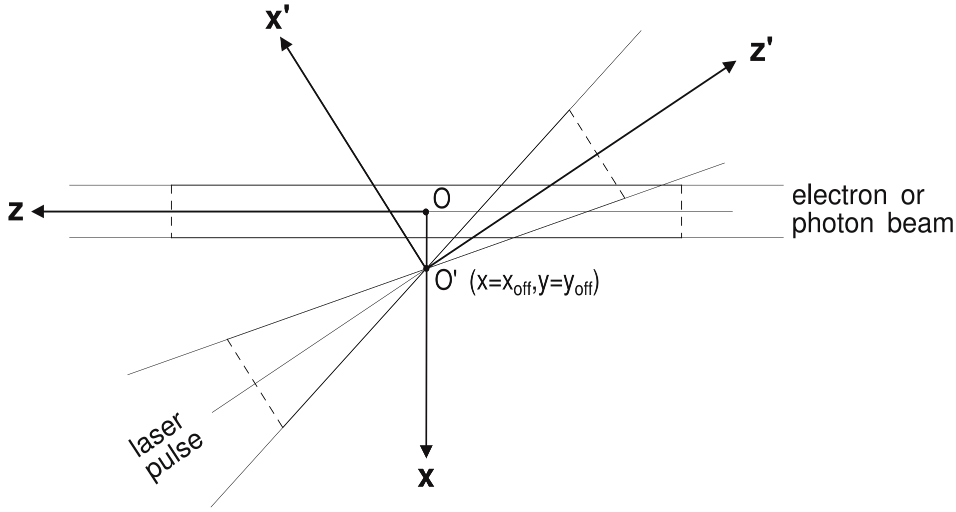

Figure 4: Coordinate Systems for modeling beam densities.

The CS (x', y', z') has the z'-axis pointing in the direction of propagation of the laser pulse and x' is lying in the plane defined by z' and the flight direction of beam particles. The center O' of the CS, *i.e.* $x' = y' = z' = 0$, is at the focus of the laser beam.

The beam density ρ_{beam} is best described in the CS (x, y, z) with z pointing along the beam and $y \parallel y'$. The origine O of (x, y, z) is such that the density of beam particles is symmetric with respect to the z-axis and O' is at $z = 0$.

In general, the two beams have a spatial offset, *i.e.* the two origines O and O' are not identical. Such an offset is introduced by the two parameters x_{off} and y_{off} which are the coordinates of O' in the CS (x, y, z). With these definitions, the transformations between the two coordinate systems are

$$
\begin{aligned}
x' &= -z \, \sin\alpha \; + \; (x - x_{\text{off}}) \cos\alpha \;, && (87)\\
y' &= y \; - \; y_{\text{off}} \;, && (88)\\
z' &= z \, \cos\alpha \; + \; (x - x_{\text{off}}) \sin\alpha \;, && (89)
\end{aligned}
$$

and

$$
\begin{aligned}
x &= z' \sin\alpha \; + \; x' \cos\alpha \; + \; x_{\text{off}} \;, && (90)\\
y &= y' \; + \; y_{\text{off}} \;, && (91)\\
z &= z' \cos\alpha \; - \; x' \sin\alpha \;. && (92)
\end{aligned}
$$

3.1 Density of Laser Photons

The waist of a diffraction limited, focused Gaussian beam propagating along z' and with a focal point a $z' = 0$ is described by the $1/e$ radius of the field intensity as a function of z' [7], *i.e.*

$$
r_0(z') = r_0 \, \sqrt{1 \; + \; (z'/z_R)^2} \;. \qquad (93)
$$

Here r_0 is the $1/e$ radius of the intensity at the focus and z_R is the Rayleigh range of the focus, given by

$$
\begin{aligned}
r_0 &= (\sqrt{2}/\pi) \; f_{\#}\lambda \;, && (94)\\
z_R &= (4/\pi) \; f_{\#}^2\lambda \;, && (95)
\end{aligned}
$$

where $f_{\#} = f/D$ is the f-number of the focusing optic and λ is the wavelength of the laser. The diffraction limited spot size at the focus is then

$$
A_0 \;\equiv\; \pi r_0^2 \;=\; (2/\pi) \; (f_{\#}\lambda)^2 \;. \qquad (96)
$$

No high power laser systems focuses perfectly to the diffraction limit [8]. For beams that are reasonably close to the diffraction limit, the primary distortion is a broadening of the Gaussian distribution near the focus. Such an effect can be included in the model of the laser focus by describing the $1/e$ radius of the field intensity as

$$
r(z') = r_0 \, \sqrt{a \; + \; (z'/z_R)^2} \;, \qquad (97)
$$

where $a = A_{\text{eff}}/A_0$ is the ratio of the effective and the diffraction limited focal spot size. The effect of a on the area $A(z')$ of the beam is then

$$A(z') \equiv \pi r(z')^2 = A_0 \left[a + (z'/z_R)^2 \right] , \tag{98}$$

which is shown in Fig. 5 for the three cases a=1, 2 and 4. The laser 'focusing angle' ξ, *i.e.* the angle between the axis of the laser beam and the tangent to the $1/e$ intensity envelope, is given by

$$\tan\xi \equiv \lim_{z'\to\infty} \frac{r(z')}{z'} = \frac{r_0}{z_R} = \frac{1}{2\sqrt{2}\, f_\#} . \tag{99}$$

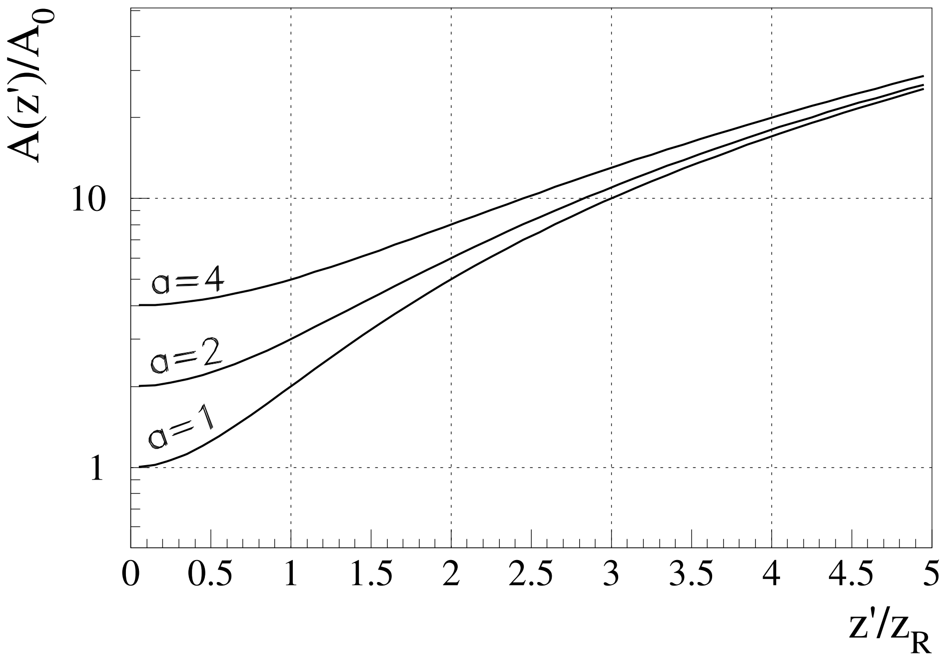

Figure 5: Beam area normalized to A_0, the diffraction limited focal spot size, as a function of z'/z_R for the three cases a=1, 2 and 4.

Defining $t = 0$ as the time at which the center of the laser pulse is at the focus, the density of laser photons as a function of space and time can be expressed in the CS (x', y', z') as

$$\rho_\omega(x', y', z', t) = \frac{N_\omega}{(2\pi)^{3/2}\, \sigma_{x'}(z')\, \sigma_{y'}(z')\, \sigma_{z'}} \exp\left[-\frac{x'^2}{2\sigma_{x'}^2(z')} - \frac{y'^2}{2\sigma_{y'}^2(z')} - \frac{(z' - \mu_{z'}(t))^2}{2\sigma_{z'}^2} \right] , \tag{100}$$

where N_ω is the total number of photons in the laser pulse and $\mu_{z'}(t) \equiv c \cdot t$ is the center of the laser pulse at time t. The widths of the focused Gaussian distribution is given by

$$\sigma_{x'}(z') = \sigma_{y'}(z') = \frac{r(z')}{\sqrt{2}} = \frac{f_\# \lambda}{\pi} \sqrt{a + (z'/z_R)^2} \qquad \text{and} \tag{101}$$

$$\sigma_{z'} = \frac{c \cdot \tau_{\text{laser}}}{2\sqrt{-\ln(1/4)}} = \frac{c \cdot \tau_{\text{laser}}}{2.355} , \tag{102}$$

where τ_{laser} is the temporal full-width-at-half-maximum of the laser pulse.

3.2 Density of Beam Particles

The particle beam colliding with the laser pulse is assumed to be cylindrical, *i.e.* not focused, and hence the widths of the Gaussian density distribution are all independent of z. Introducing a possible time delay t_{off} of the laser pulse with respect to the beam (or a time advance of the beam w.r.t. the laser pulse), the beam particle density as a function of space and time in the CS (x, y, z) is

$$\rho_{\text{beam}}(x, y, z, t) = \frac{N_{\text{beam}}}{(2\pi)^{3/2}\, \sigma_x\, \sigma_y\, \sigma_z} \exp\left[-\frac{x^2}{2\sigma_x^2} - \frac{y^2}{2\sigma_y^2} - \frac{(z - \mu_z(t + t_{\text{off}}))^2}{2\sigma_z^2}\right] , \tag{103}$$

where N_{beam} is the total number of beam particles and $\mu_z(t + t_{\text{off}}) \equiv c \cdot (t + t_{\text{off}})$ is the center of the beam at time t. Again, the width σ_z is related to the temporal full-width-at-half-maximum τ_{beam} by

$$\sigma_z = \frac{c \cdot \tau_{\text{beam}}}{2\sqrt{-\ln(1/4)}} = \frac{c \cdot \tau_{\text{beam}}}{2.355} . \tag{104}$$

3.3 Energy Spectra

The laser beam is assumed to consist of monoenergetic photons and experimental situations where more than one laser color is sent to the IP are not supported in the simulation (I don't know whether a consistent theoretical model exists for this type of interactions).

The electron beam is also assumed to be monoenergetic in the current version of NI. However, this is not a fundamental assumption and the program could easily be extended to handle an electron beam with a spectrum of energies.

For a photon-laser collision, three types of energy spectra are supported, namely a monoenergetic spectrum, a Compton spectrum and a bremsstrahlung spectrum. The Compton spectrum is read from the 'log-file' of a previous simulation of an electron-laser collision and therefore can include the effects of Compton scattering in a strong field, *i.e.* multiphoton interactions, multiple interactions and mass shift.

The bremsstrahlung spectrum describes a photon beam created by inserting a thin foil in a monoenergetic electron beam upstream of the IP. For clean photon-laser interactions, the charged particles in the beam (beam electrons, scattered electrons and positrons) need to be deflected out of the photon beam line between the foil and the IP. The bremsstrahlung spectrum is calculated according to Ref. [9], formula 3CS(a), which is valid in the extreme relativistic region and takes into account 'Coulomb corrections' and 'complete screening'. The number of bremsstrahlung photons with energy ω' is given by

$$\frac{dN(\omega')}{d\omega'} = N_e \cdot \rho_t \cdot d \cdot \frac{d\sigma(\omega')}{d\omega'}, \tag{105}$$

where N_e is the number of electrons incident on the foil, ρ_t is the density of target nuclei, d is the thickness of the foil and the differential cross-section for bremsstrahlung is

$$d\sigma(\omega') = 4Z^2 r_0^2 \alpha \cdot \frac{d\omega'}{\omega'} \left\{ \left[1 + \left(\frac{E}{E_0} \right)^2 - \frac{2}{3} \frac{E}{E_0} \right] \left[\ln \left(183 Z^{-1/3} \right) - 1.2021 (Z\alpha)^2 \right] + \frac{1}{9} \frac{E}{E_0} \right\} , \tag{106}$$

where E_0 and $E = E_0 - \omega'$ are the initial and final electron energies, Z is the atomic number of the foil material, $r_0 = e^2/mc^2$ is the classical electron radius and $\alpha = e^2/\hbar c$ is the fine structure constant.

4 Integration over Space and Time

For a numeric integration of nonlinear QED processes in electron-laser or photon-laser collisions, space and time are divided in small elements. The yields of interactions between the particle beam and the laser field are calculated for each of these space-time elements (STE) according to the formulas presented in Sec. 2 and are then combined to the total interaction results. I will refer to the beam-laser interactions a the 'primary processes'.

The results of the processes presented in Sec. 2 are then calculated for each of these space-time elements (STE) and later combined.

In this approach it is assumed that the particle densities (both laser and beam) are constant within a STE. Therefore, the integration grid defining the elements must be chosen in such a way that the particle densities have little variation within a STE.

For an accurate and efficient calculation, the choice of the grid should account for the focusing of the laser beam, *i.e.* the space-time elements close to the laser focus must be smaller than those far away from the focal point.

It is natural to define the integration grid in the laser CS (x', y', z') and in units of $\sigma_{x'}(z')$, $\sigma_{y'}(z')$ and $\sigma_{z'}$ as defined in Eq. (101) and (102). The following parameters specify the grid in space:

$n^\sigma_{x'}$, $n^\sigma_{y'}$, $n^\sigma_{z'}$: size of integration volume in x', y', z' in units of Gaussian sigmas,
$n^\Delta_{x'}$, $n^\Delta_{y'}$, $n^\Delta_{z'}$: number of elements in integration volume along x', y', z'.

With these parameters, the spatial volume of an STE is given by

$$dV(z') \equiv dx'(z') \cdot dy'(z') \cdot dz' = \frac{2\, n^\sigma_{x'}\, \sigma_{x'}(z')}{n^\Delta_{x'}} \cdot \frac{2\, n^\sigma_{y'}\, \sigma_{y'}(z')}{n^\Delta_{y'}} \cdot \frac{2\, n^\sigma_{z'}\, \sigma_{z'}}{n^\Delta_{z'}} . \tag{107}$$

Note that the size of a STE along z' can be constant (see Sec. 9 for variable step sizes in z' and time). However, along x' and y' the element size is not constant but depends on z'. This is shown in Fig. 6 for $n^\sigma_{x'} = n^\sigma_{z'} = 3$ and $n^\Delta_{x'} = n^\Delta_{z'} = 8$. The step-size in time should be comparable to dz', *i.e.* $c \cdot dt \sim dz'$, and can be specified by the ratio

$$R^{dt}_{dz'} \equiv \frac{c\, dt}{dz'} . \tag{108}$$

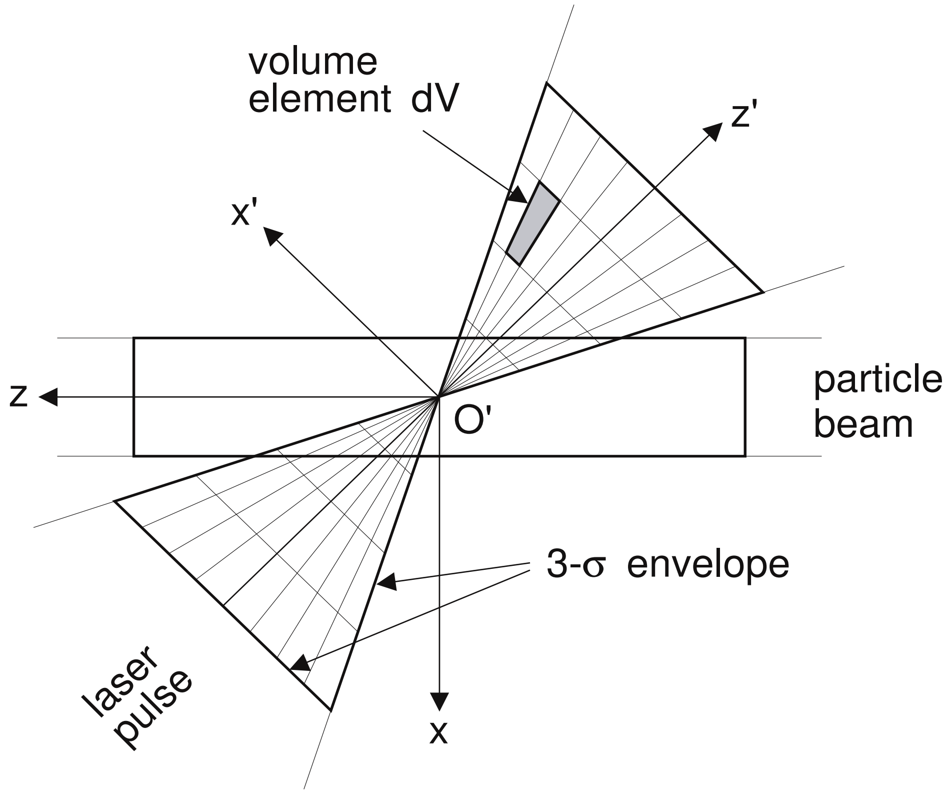

Figure 6: Space-Time grid in the $x'z'$-plane for $n_{x'}^{\sigma} = n_{z'}^{\sigma} = 3$ and $n_{x'}^{\Delta} = n_{z'}^{\Delta} = 8$.

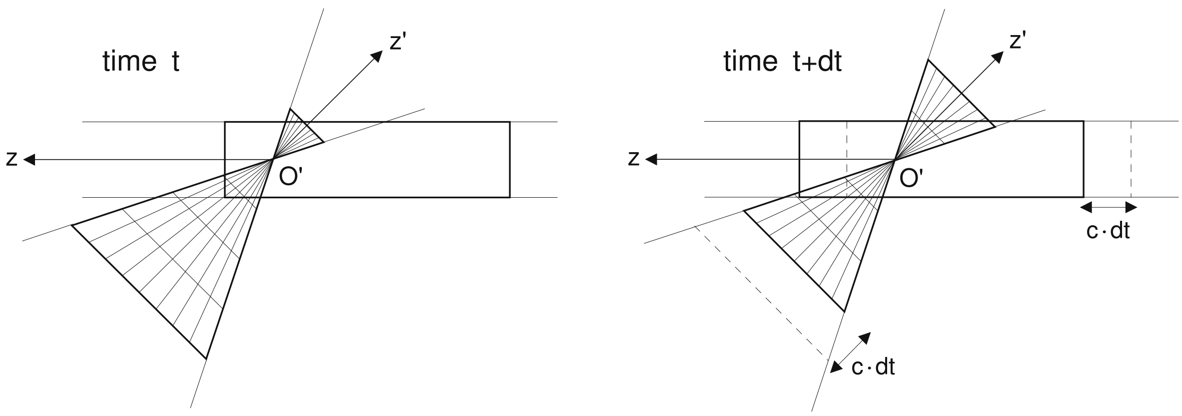

Figure 7: Spatial integration grid at two consecutive time steps.

The integration over space and time for a process X (*e.g.* NLCS or MPBW) proceeds then in the following way:

1. For a given time t, loop over all volume elements dV in the integration grid.

2. For each volume element, calculate the interaction rate W_X according to Sec. 2 and obtain the interaction yield as

$$N_\mathrm{X}^{STE} = W_\mathrm{X} \cdot dV \cdot dt \, . \tag{109}$$

3. Update the total interaction yield for process X, i.e.

$$N_\mathrm{X}^{total} + = N_\mathrm{X}^{STE} \, . \tag{110}$$

4. Advance time by dt, *i.e.* move both beams forward by $c \cdot dt$ and start over at 1.

Figure 7 shows the spatial integration grid for two consecutive time steps at t and $t + dt$.

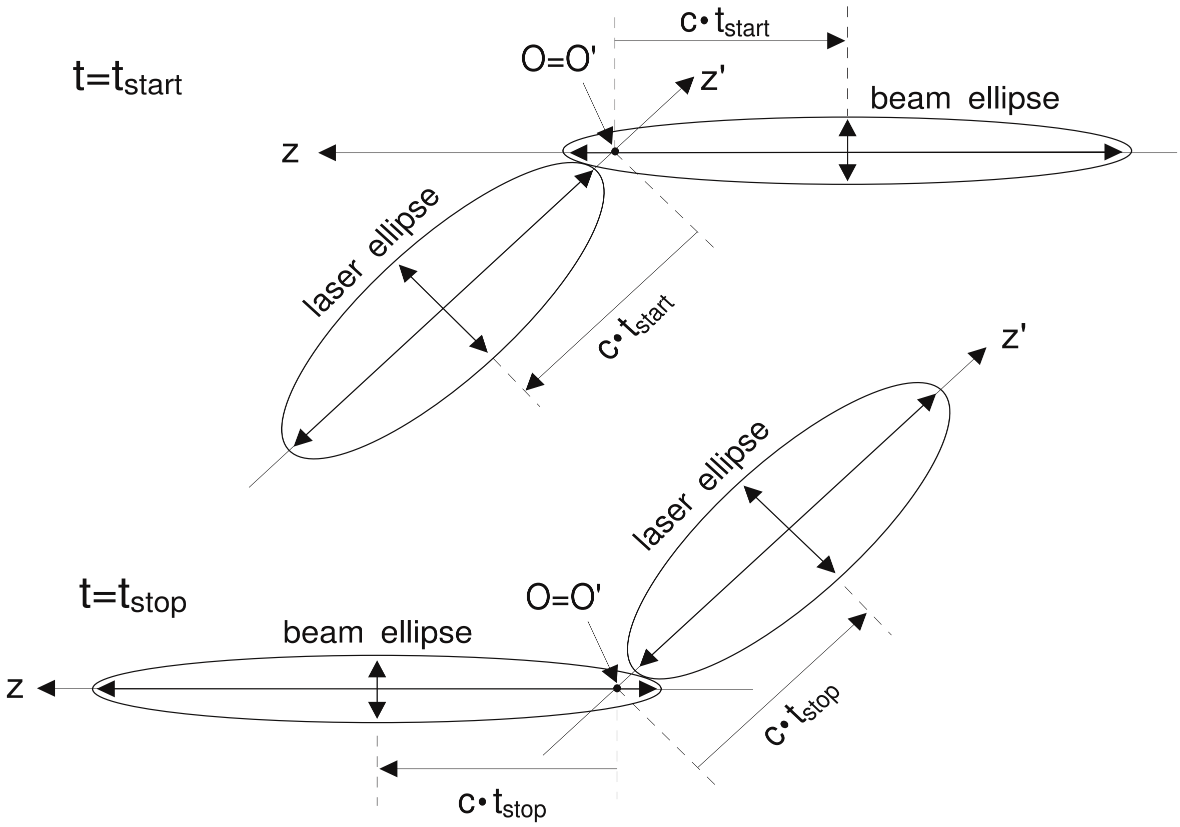

Figure 8: Procedure to find t_start and t_stop, the beginning and end of spatial overlap between the two beams. The drawings include no temporal and spatial offsets between the two beams.

The integration range in time is given by t_start and t_stop which are defined by the beginning and end of spatial overlap between the two beams (or better the $n - \sigma$ envelopes of the beams). The procedure implemented in NI to find t_start and t_stop is explained in Fig. 8. It approximates the beam envelopes in the xz-plane as ellipses. The half-axis parallel (a) and perpendicular (b) to the beam directions are given by

$$
\begin{aligned}
a_{\text{laser}} &= n^{\sigma}_{z'} \cdot \sigma_{z'} \ , && (111)\\
b_{\text{laser}} &= n^{\sigma}_{x'} \cdot \sigma_{x'}(z'_{max}) \ , && (112)\\
a_{\text{beam}} &= n^{\sigma}_{z'} \cdot \sigma_{z} \ , && (113)\\
b_{\text{beam}} &= n^{\sigma}_{x'} \cdot \sigma_{x} \ . && (114)
\end{aligned}
$$

where z'_{max} is the distance between the laser focus and the far end of the laser ellipse (*i.e.* $\sigma_{x'}$ is taken at maximum size for z' within the ellipse). The two ellipses are first positioned for $t = 0$, taking into account t_{off} and x_{off}, *i.e.* possible temporal and spatial offsets between the two beams. Then, the ellipses are moved along z and z' in positive and negative directions until they have no common area. The distance from this points to the original position is then $c \cdot t_{\text{start}}$ and $c \cdot t_{\text{stop}}$.

This algorithm tends to overestimate the integration range in time and also does not account for a possible spatial offset in y, which would further limit the time range. Improved procedures or even completely or partially analytic solutions of this problem are certainly conceivable. However, due to the speed optimizations mentioned later in Sec. 9, a slight overestimation of the time range has only a very minor effect on the CPU time required for a simulation.

5 Secondary Processes

The final state particles of reactions calculated for a STE are usually still within the laser field and can undergo further interactions. These ‘secondary processes’ can be important and need to be accounted for in a realistic simulation. For example, in an experimental setup like E-144, the yield of electrons below the linear ($n = 1$) Compton edge has comparable contributions from double ordinary Compton scattering and nonlinear Compton scattering with $n = 2$. Even more dramatic, the pair production in electron-laser collisions, as measured by E-144, seems to be completely dominated by the secondary Breit-Wheeler process. Here Compton backscattered laser photons (primary process) undergo multiphoton interactions with the laser field (secondary process) to produce e^+e^- pairs.

In the program NI, secondary processes are taken into account by an additional integration over time t' for each space-time element. Figure 9 shows this secondary integration, where the volume element dV has a fixed size and moves along the beam axis z while the laser pulse continues to propagate along the z' axis as time evolves. The direction of motion and the fixed size of the volume element dV are based on the assumption that all final state particles move along z in the LAB frame. This is motivated by the fact that final state particles of the reactions considered emerge from the reaction point with typical angles of order $1/\gamma$ with respect to the incoming beam. Therefore, in an experimental setup like E-144 where γ is of order 10^5, this assumption is certainly justified.

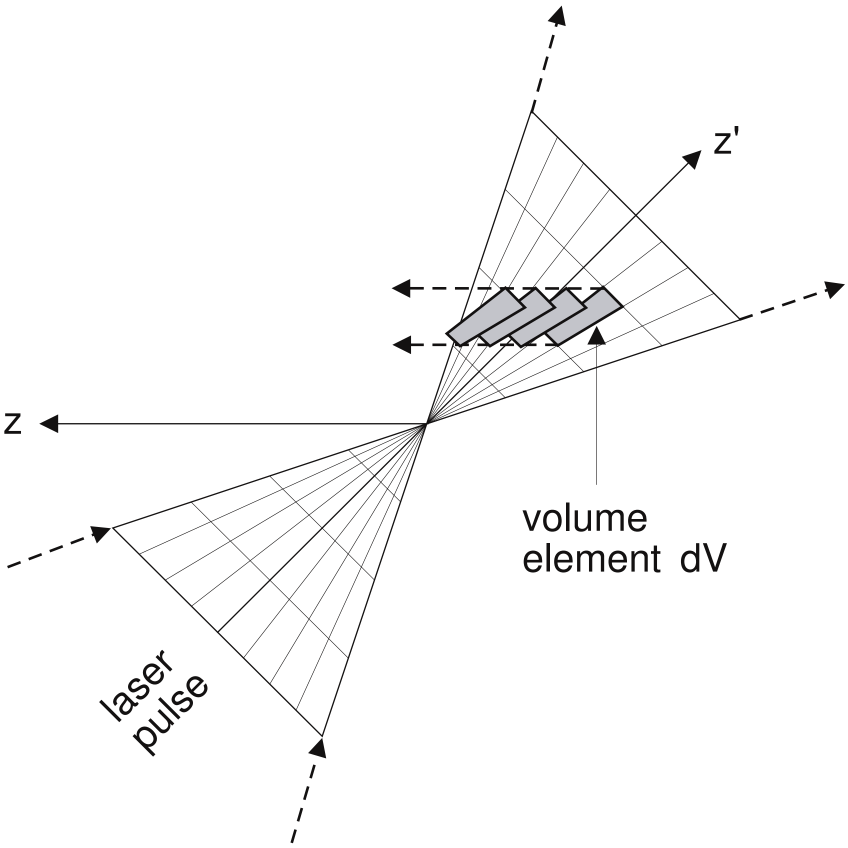

Figure 9: Integration over time for secondary processes. The volume element dV is moved along the beam axis z while the laser pulse continues to propagate along z'.

The step-size $c \cdot dt'$ during the secondary integration should be comparable to the linear dimensions of the spatial grid at the current location $(x'_{\mathrm{s}}, y'_{\mathrm{s}}, z'_{\mathrm{s}})$ of dV. Figure 10 explaines the procedure implemented in NI to calculate the secondary step-size $c \cdot dt'$, which is given by the formula

$$c \cdot dt'(x'_{\mathrm{s}}, y'_{\mathrm{s}}, z'_{\mathrm{s}}) = \min\left[c \cdot dt'_1(x'_{\mathrm{s}}, y'_{\mathrm{s}}, z'_{\mathrm{s}}), c \cdot dt'_2(x'_{\mathrm{s}}, y'_{\mathrm{s}}, z'_{\mathrm{s}})\right] \;, \tag{115}$$

where

$$c \cdot dt'_1(x'_{\mathrm{s}}, y'_{\mathrm{s}}, z'_{\mathrm{s}}) = \frac{dz'(x'_{\mathrm{s}}, y'_{\mathrm{s}}, z'_{\mathrm{s}})}{|\cos\alpha|} \;, \tag{116}$$

$$c \cdot dt'_2(x'_{\mathrm{s}}, y'_{\mathrm{s}}, z'_{\mathrm{s}}) = \frac{dx'(x'_{\mathrm{s}}, y'_{\mathrm{s}}, z'_{\mathrm{s}})}{|\sin\alpha|} \;, \tag{117}$$

and $dx'(x'_{\mathrm{s}}, y'_{\mathrm{s}}, z'_{\mathrm{s}})$, $dz'(x'_{\mathrm{s}}, y'_{\mathrm{s}}, z'_{\mathrm{s}})$ are defined in Eq. (107). Note that with this procedure the step-size adjusts to the spatial grid-size as the volume element dV' moves out of the laser field.

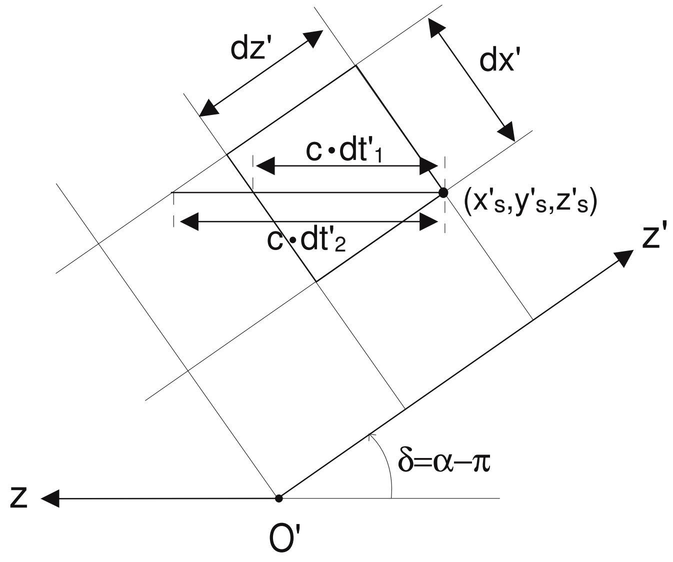

Figure 10: Procedure to calculate the step-size for the secondary integration over time.

The secondary integration starts at the original location of the (primary) STE. However, only half the step-size in time is used in the calculation of secondary reaction yields for the first step, accounting for the fact that on average the secondary particles become available only after the first half of the time step.

The integration over t' can be stoped when dV has left the laser field and no further interactions are expected. The criterion implemented in NI to stop the integration requires the product $P_{\eta 2dV} \equiv \eta^2 \cdot dV$ for the secondary STE to drop below a certain threshold, *i.e.*

$$P_{\eta 2dV} < F_{\eta 2dV} \cdot P_{\eta 2dV}^{\max} , \tag{118}$$

where $P_{\eta 2dV}^{\max}$ is the maximum of $P_{\eta 2dV}$ for all primary STEs and $F_{\eta 2dV}$ is an input parameter to the numeric integration.

For crossing angles $\delta = \alpha - \pi$ comparable to or smaller than the laser focusing angle ξ as defined in Eq. (99), it is possible for a volume element dV to leave and later reenter the laser field as demonstrated in Fig. 11. However, the criterion given in Eq. (118) will stop the integration as soon as dV has left the laser field and the progam NI will not account for the additional interactions that occur when dV reenters the field. This is not of concern for the interaction geometry of E-144 where $\delta = 17$ degrees and $\xi \simeq 3.4$ degrees. Nevertheless, the user should be aware of this limitation and an improved version of NI should use a criterion for terminating the secondary integration that can handle these cases correctly.

Note that the procedure described above to calculate secondary processes ignores interactions between the final state particles and beam electrons.

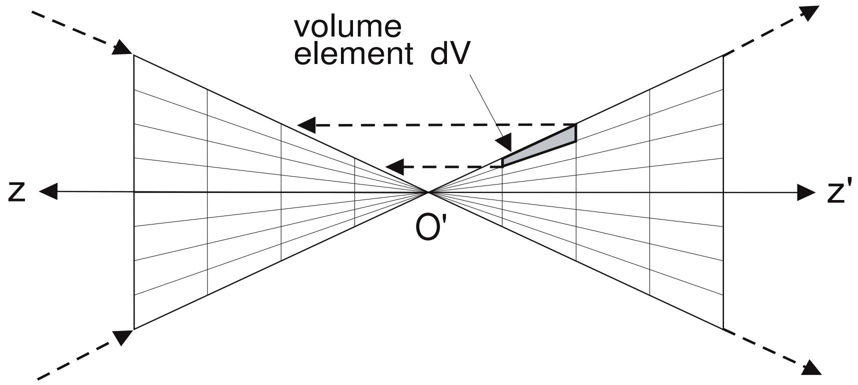

Figure 11: For small crossing angles between the laser and the primary beam, a volume element dV may first leave and later reenter the laser field along the path of secondary time integration.

6 Program Flow

The program execution flow for the simulation of a single beam-laser interaction is shown in Fig. 12. The calculation consists of three main parts, namely the initialization, the actual integration and the termination.

During the initialization part, unknown parameters are calculated from input parameters or read from external files, memory is allocated, counters are initialized and all input parameters and program options are written to the ‘log-file’. Some of the steps shown in the diagram of Fig. 12 are executed only if certain program options are selected and will be discussed in the following sections.

In the actual integration, the program calls first the analysis initialization routine and then loops over all space-time elements. For each STE, the primary processes (P1_X) selected by the program options are calculated, the results are analyzed and the particle spectra for this STE are updated. Then follows the additional integration over time where for each secondary STE the selected secondary processes (P2_X) are calculated, the results analyzed and the particle spectra updated. Finally, the results for this (primary) STE, including secondary processes, are analyzed and added to the total results of the collision. The integration part ends with a call to a final analysis routine.

The calculation of either a primary or secondary process consists usually of an additional three loops, *i.e.* the initial particle energy, the number of laser photons in the interaction and the final particle energy. For primary processes, the initial particle energy may be monoenergetic and only two loops are needed. At the center of these loops, all parameters needed for the formulas of Sec. 2 are finally defined. The reaction yield is evaluated and analyzed and process specific spectra and counters are updated.

In the final program part, results are written to the ‘log-file’, histograms are saved to the histogram file and the allocated memory is freed.

The program provides various entry points for a user specific analysis of the simulation.

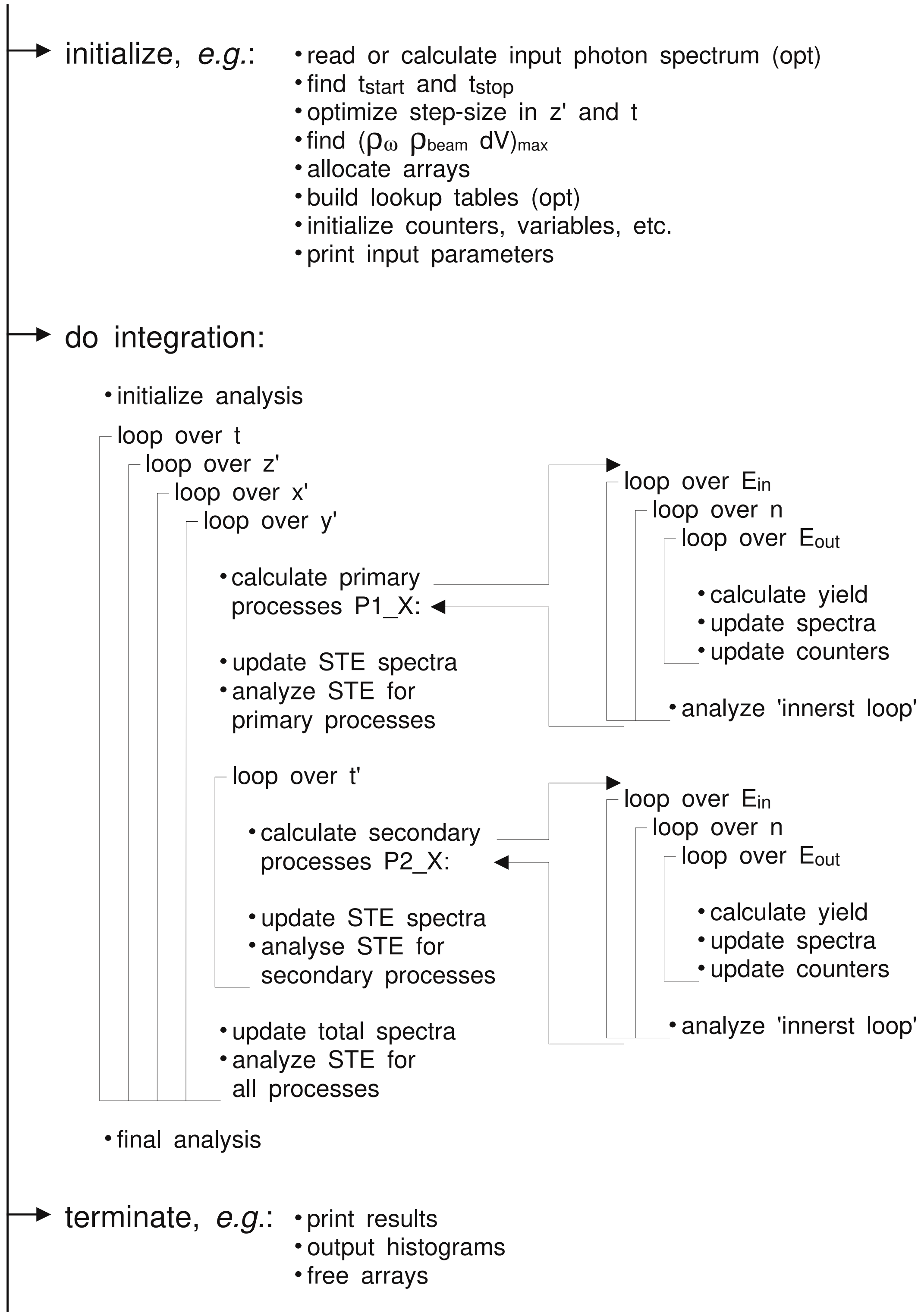

Figure 12: Schematic diagram of program execution flow.

Histograms can be booked in the analysis initialization routine. The STE analysis following the calculation of primary processes allows to analyze the results of only primary processes in the current (primary) STE. Similarly, the analysis calls during the secondary integration over time allow to analyze secondary processes for each secondary STE. In the last analysis call for a STE, the results from primary and all secondary processes are combined. The most detailed information is provided by the 'innerst loop' analysis which is called from the calculation of each primary and secondary processe.

Since the STE analysis and especially the 'innerst loop' analysis calls can considerably slow down program execution, all types of analysis are selectable as program options.

7 Saving Results

The program NI maintains a set of defaults counters and particle spectra to store the results of the simulation. These objects are defined globally in NI and can be accessed from any routine. While some of the spectra are actually needed for further calculations, most of these spectra and counters are provided as a simple and standardized way to summarize results and to present these results in the 'log-file'. More sophisticated analysis can be performed in user supplied analysis routines.

A spectrum is stored as an array `sp[..]` of dimension m with an array index i in the range $[0, m-1]$. Each element of the array represents an energy bin of width $\Delta E = E_{\max}/m$ with $E_{\max}$ the upper limit of the spectrum. All spectra in the simulation have identical dimensions d and bin widths ΔE (with one exception, see below).

However, for reasons explained below, the spectra for photons and e^+e^- pairs are shifted by half a bin with respect to the spectra for electrons and positrons. For electron and positron spectra, the bin with index i has a center energy E^i_{cen}, a lower limit E^i_{low} and an upper limit E^i_{high} given by

$$\begin{aligned} E^i_{\text{cen}} &= (i - 1/2) \cdot \Delta E \,, \\ E^i_{\text{low}} &= i \cdot \Delta E \,, \\ E^i_{\text{high}} &= (i + 1) \cdot \Delta E \,, \end{aligned} \tag{119}$$

while for photon and e^+e^- pair spectra these values are

$$\begin{aligned} E^i_{\text{cen}} &= i \cdot \Delta E \,, \\ E^i_{\text{low}} &= (i - 1/2) \cdot \Delta E \,, \\ E^i_{\text{high}} &= (i + 1/2) \cdot \Delta E \,, \end{aligned} \tag{120}$$

with the exception of the first bin where the effective bin width is $\Delta E_{\text{eff}} = \Delta E/2$ and the lower limit is $E^0_{\text{low}} = 0$.

The reason for this shift is that in all processes simulated by NI three particles are involved in addition to the laser photons, but only two can have an energy at the center of a bin and the third one will end up at a bin boundary of a spectrum not shifted. As an example, consider the secondary Compton scattering process for electrons with an initial energy $E^i_{\rm cen} = (i - 1/2) \cdot \Delta E$ and a final energy $E^j_{\rm cen} = (j - 1/2) \cdot \Delta E$. The energy of the scattered photon is then

$$E^k = E^i_{\rm cen} - E^j_{\rm cen} = (i - j) \cdot \Delta E, \tag{121}$$

which is at a bin boundary for a spectrum not shifted.

7.1 Combined Results

As already indicated in the previous section, many processes are usually active during a simulation and they are not independent from each other, *i.e.* the results of one process serve as the input to another process. For example, the Compton backscattered photon beam is the input to the multiphoton Breit-Wheeler pair production and the electrons and positrons produced in this interaction will undergo further Compton scatters *etc.*

The following processes can be selected for a simulation of nonlinear QED (NLQED) processes in electron-laser or photon-laser collisions:

P1_NLCS : primary nonlinear Compton scattering,
P1_BW : primary multiphoton Breit-Wheeler pair production,
P1_WWBW : primary multiphoton trident pair production,

P2_NLCS : secondary nonlinear Compton scattering,
P2_BW : secondary multiphoton Breit-Wheeler pair production,
P2_WWBW : secondary multiphoton trident pair production.

The main results of such a simulation are summarized by the energy spectra of all photons, electrons and positrons produced in the collision. These spectra contain now the contributions from all selected processes and can be compared to experimental measurements.

For NLQED processes, the program keeps also track of the energy spectrum of e^+e^- pairs and the photon polarization spectrum, *i.e.* the polarization of the backscattered photon beam as a function of the photon energy. The list of spectra calculated by NI for NLQED processes is then:

`phsp_nl[..]` : total photon energy spectrum (NLQED),
`elsp_nl[..]` : total electron energy spectrum (NLQED),
`posp_nl[..]` : total positron energy spectrum (NLQED),
`pasp_nl[..]` : total e^+e^- pair energy spectrum (NLQED),
`phpo_nl[..]` : total photon polarization spectrum (NLQED).

The Klein-Nishina approximation to Compton scattering (KNCS) is treated as an independent group of interactions with only two processes, namely

P1_KNCS : primary Klein-Nishina scattering and
P1_KNCS : secondary Klein-Nishina scattering.

Results from these two processes are kept separate from those of NLQED calculations in the two spectra

`phsp_kn[..]`	: photon energy spectrum (KNCS) and
`elsp_kn[..]`	: electron energy spectrum (KNCS).

Since NLQED and KNCS processes are completely independent, the two types of simulations can be run simultaneously in NI, *e.g.* it is valid to select P1_NLCS and P1_KNCS.

A third group of processes are the interactions of electrons, positrons and photons with a static electromagnetic field. Here the processes are primary and secondary 'beamstrahlung' and 'coherent pair production' and they are complementary to the NLQED processes. However, as mentioned in the introduction, this type of interactions are not documented in this write-up.

The calculations for a (primary) STE are independent from all other STEs and therefore the total particle spectra are the sum of the spectra for individual STEs, *i.e.* for NLQED processes

$$\texttt{xxsp\_nl}[..] = \sum_{\text{STEs}} \texttt{stp\_xxsp\_nl}[..] \;, \tag{122}$$

where the list of spectra for NLQED processes specific to a STE is

`stp_phsp_nl[..]`	: photon energy spectrum for STE (NLQED),
`stp_elsp_nl[..]`	: electron energy spectrum for STE (NLQED),
`stp_posp_nl[..]`	: positron energy spectrum for STE (NLQED),
`stp_pasp_nl[..]`	: e^+e^- pair energy spectrum for STE (NLQED),
`stp_phpo_nl[..]`	: photon polarization spectrum for STE (NLQED).

Figure 13 shows how the spectra specific to a STE are updated by the various processes in the simulation. As an example, consider the secondary Compton scattering process (P2_NLCS) for electrons with an initial energy E^i and a final energy E_j. The energy of the scattered photon is then $E^k = E^i - E^j$ and the spectra bins corresponding to the energies E^i, E^j and E^k are labeled as `[i]`, `[j]` and `[k]`. The input to P2_NLCS is `stp_elsp_nl[i]`, *i.e.* the number of secondary electrons in this STE with energy E^i. For a reaction yield of N_{ij} Compton scatters and a fraction of $P(E^k) = N_{ij}^{\|}/N_{ij}$ backscattered photons with a polarization parallel to the laser field, the photon polarization spectrum as defined in Eq. (37) is updated according to

$$\texttt{stp\_phpo\_nl}[\texttt{k}] \rightarrow \frac{\texttt{stp\_phpo\_nl}[\texttt{k}] \times \texttt{stp\_phsp\_nl}[\texttt{k}] \;+\; N_{ij}^{\|}}{\texttt{stp\_phsp\_nl}[\texttt{k}] + N_{ij}} \;, \tag{123}$$

and the energy spectra as

$$\texttt{stp\_elsp\_nl}[\texttt{i}] \;\rightarrow\; \texttt{stp\_elsp\_nl}[\texttt{i}] \;-\; N_{ij} \;, \tag{124}$$

$$\texttt{stp\_elsp\_nl}[\texttt{j}] \;\rightarrow\; \texttt{stp\_elsp\_nl}[\texttt{j}] \;+\; N_{ij} \;, \tag{125}$$

$$\texttt{stp\_phsp\_nl}[\texttt{k}] \;\rightarrow\; \texttt{stp\_phsp\_nl}[\texttt{k}] \;+\; N_{ij} \;. \tag{126}$$

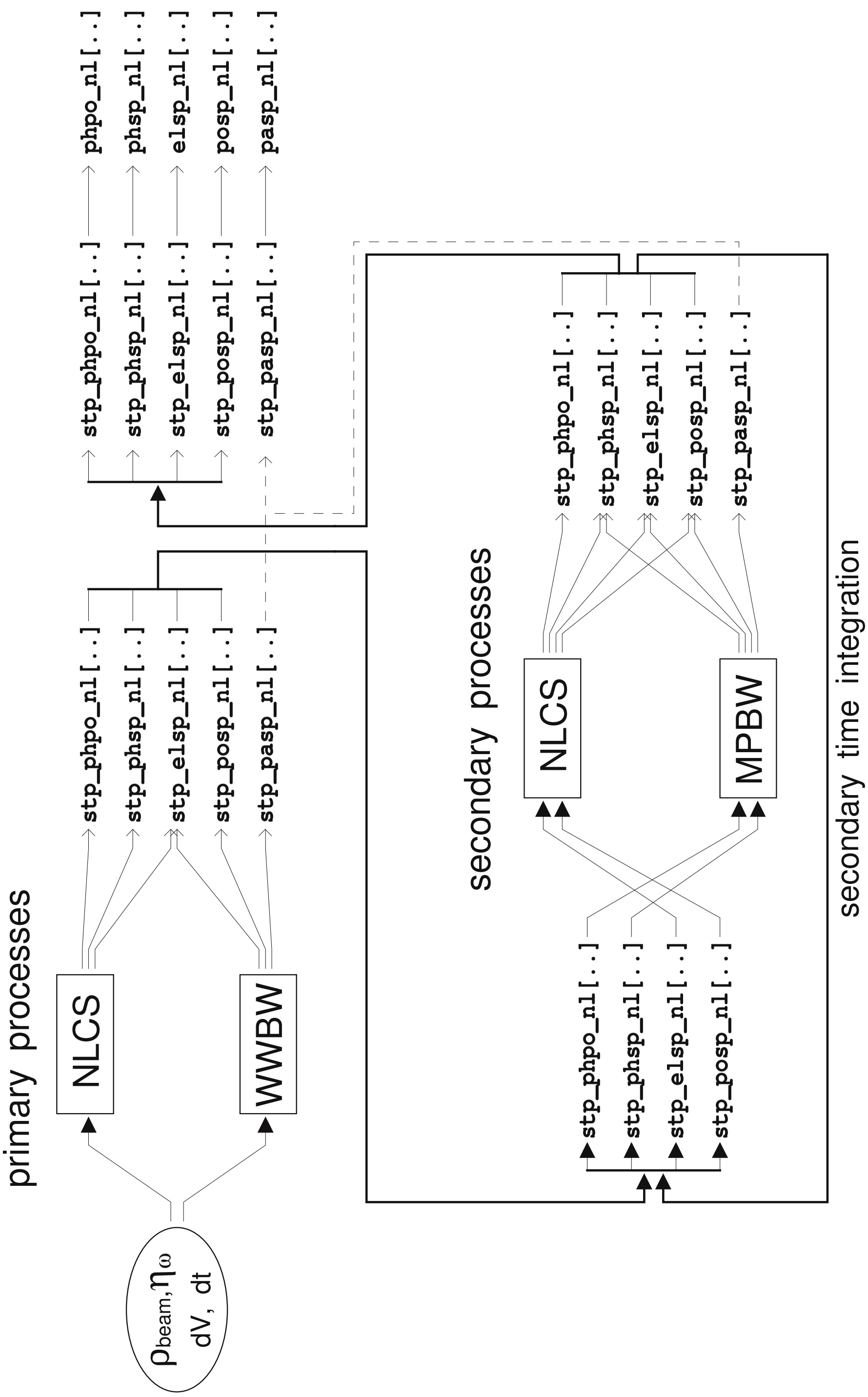

Figure 13: Demonstration of updating the STE particle spectra at the example of an electron-laser interaction including the processes P1_NLCS, P1_WWBW, P2_NLCS and P2_MPBW.

Note that the single particle energy spectra and the photon polarization spectrum are updated not only for particles created in interactions (see Eq. (125)) but also for particles spent in these process (see Eq. (124)). I will refer to this type of spectra as *active* or *updating*. However, since the correlation between the electron and the positron of a pair is lost in the single particle spectra that serve as input to further processes, the pair spectrum `stp_pasp_nl[..]` keeps only track of pairs created in interactions. This is a first example of a *passive* or *accumulating* spectrum.

Besides the particle spectra mentioned above, the numeric integration NI provides a set of counters that keep track of the total number and energy of particles created in interactions with n laser photons, *i.e.* interactions of order n. These counters are all *passive* and for NLQED processes they are denoted by

`phnr_nl_n[..]`	: total number of photons from order n interactions (NLQED),
`elnr_nl_n[..]`	: total number of electrons from order n interactions (NLQED),
`ponr_nl_n[..]`	: total number of positrons from order n interactions (NLQED),
`panr_nl_n[..]`	: total number of e^+e^- pairs from order n interactions (NLQED),
`phene_nl_n[..]`	: total energy of photons from order n interactions (NLQED),
`elene_nl_n[..]`	: total energy of electrons from order n interactions (NLQED),
`poene_nl_n[..]`	: total energy of positrons from order n interactions (NLQED),
`paene_nl_n[..]`	: total energy of e^+e^- pairs from order n interactions (NLQED).

The total number and energy of particles, independent of the interaction order, is given by

`phnr_nl_tot`	: total number of photons from all orders (NLQED),
`elnr_nl_tot`	: total number of electrons from all orders (NLQED),
`ponr_nl_tot`	: total number of positrons from all orders (NLQED),
`panr_nl_tot`	: total number of e^+e^- pairs from all orders (NLQED),
`phene_nl_tot`	: total energy of photons from all orders (NLQED),
`elene_nl_tot`	: total energy of electrons from all orders (NLQED),
`poene_nl_tot`	: total energy of positrons from all orders (NLQED),
`paene_nl_tot`	: total energy of e^+e^- pairs from all orders (NLQED).

As mentioned above, the results for the Klein-Nishina approximation to Compton scattering are kept separate from the NLQED results. Besides the two main particle spectra `phsp_kn[..]` and `elsp_kn[..]` listed above, the following counters and spectra are updated by NI:

`stp_phsp_kn[..]`	: photon energy spectrum for STE (KNCS),
`stp_elsp_kn[..]`	: electron energy spectrum for STE (KNCS),
`phnr_kn_tot`	: total number of photons (KNCS),
`elnr_kn_tot`	: total number of electrons (KNCS),
`phene_kn_tot`	: total energy of photons (KNCS),
`elene_kn_tot`	: total energy of electrons (KNCS).

7.2 Process Specific Results

In addition to the spectra and counters that combine the results from all selected processes, the numeric integration keeps track of spectra and counters specific to a certain interaction. However, because the interaction history of particles is lost in the particle spectra, all process specific counters and spectra are *passive*.

For nonlinear Compton scattering (NLCS), the process specific spectra and counters are

`phsp_nlcs[..]`	: total photon energy spectrum (NLCS),
`elsp_nlcs[..]`	: total electron energy spectrum (NLCS),
`posp_nlcs[..]`	: total positron energy spectrum (NLCS),
`stp_phsp_nlcs[..]`	: photon energy spectrum for STE (NLCS),
`stp_elsp_nlcs[..]`	: electron energy spectrum for STE (NLCS),
`stp_posp_nlcs[..]`	: positron energy spectrum for STE (NLCS),
`phnr_nlcs_n[..]`	: total number of photons from order n interactions (NLCS),
`elnr_nlcs_n[..]`	: total number of electrons from order n interactions (NLCS),
`ponr_nlcs_n[..]`	: total number of positrons from order n interactions (NLCS),
`phene_nlcs_n[..]`	: total energy of photons from order n interactions (NLCS),
`elene_nlcs_n[..]`	: total energy of electrons from order n interactions (NLCS).
`poene_nlcs_n[..]`	: total energy of positrons from order n interactions (NLCS).
`phnr_nlcs_tot`	: total number of photons from all orders (NLCS),
`elnr_nlcs_tot`	: total number of electrons from all orders (NLCS),
`ponr_nlcs_tot`	: total number of positrons from all orders (NLCS),
`phene_nlcs_tot`	: total energy of photons from all orders (NLCS),
`elene_nlcs_tot`	: total energy of electrons from all orders (NLCS),
`poene_nlcs_tot`	: total energy of positrons from all orders (NLCS).

Similarly, for the multiphoton Breit-Wheeler pair production (MPBW), the process specific spectra and counters are

`phsp_bw[..]`	: total photon energy spectrum (MPBW),
`elsp_bw[..]`	: total electron energy spectrum (MPBW),
`posp_bw[..]`	: total positron energy spectrum (MPBW),
`pasp_bw[..]`	: total e^+e^- pair energy spectrum (MPBW),
`stp_phsp_bw[..]`	: photon energy spectrum for STE (MPBW),
`stp_elsp_bw[..]`	: electron energy spectrum for STE (MPBW),
`stp_posp_bw[..]`	: positron energy spectrum for STE (MPBW),
`stp_pasp_bw[..]`	: e^+e^- pair energy spectrum for STE (MPBW),
`ponr_bw_n[..]`	: total number of positrons from order n interactions (MPBW),
`panr_bw_n[..]`	: total number of e^+e^- pairs from order n interactions (MPBW),
`poene_bw_n[..]`	: total energy of positrons from order n interactions (MPBW),

`paene_bw_n[..]`	: total energy of e^+e^- pairs from order n interactions (MPBW),
`ponr_bw_tot`	: total number of positrons from all orders (MPBW),
`panr_bw_tot`	: total number of e^+e^- pairs from all orders (MPBW),
`poene_bw_tot`	: total energy of positrons from all orders (MPBW),
`paene_bw_tot`	: total energy of e^+e^- pairs from all orders (MPBW).

And finally, for the multiphoton trident pair production (WWBW), the process specific spectra and counters are

`phsp_wwbw[..]`	: total photon energy spectrum (WWBW),
`elsp_wwbw[..]`	: total electron energy spectrum (WWBW),
`posp_wwbw[..]`	: total positron energy spectrum (WWBW),
`pasp_wwbw[..]`	: total e^+e^- pair energy spectrum (WWBW),
`stp_phsp_wwbw[..]`	: photon energy spectrum for STE (WWBW),
`stp_elsp_wwbw[..]`	: electron energy spectrum for STE (WWBW),
`stp_posp_wwbw[..]`	: positron energy spectrum for STE (WWBW),
`stp_pasp_wwbw[..]`	: e^+e^- pair energy spectrum for STE (WWBW),
`ponr_wwbw_n[..]`	: total number of positrons from order n (WWBW),
`panr_wwbw_n[..]`	: total number of e^+e^- pairs from order n (WWBW),
`poene_wwbw_n[..]`	: total energy of positrons from order n (WWBW),
`paene_wwbw_n[..]`	: total energy of e^+e^- pairs from order n (WWBW),
`ponr_wwbw_tot`	: total number of positrons from all orders (WWBW),
`panr_wwbw_tot`	: total number of e^+e^- pairs from all orders (WWBW),
`poene_wwbw_tot`	: total energy of positrons from all orders (WWBW),
`paene_wwbw_tot`	: total energy of e^+e^- pairs from all orders (WWBW).

8 Second Order Corrections

8.1 Effective Crossing Angle

While the crossing angle between the particle and the laser beam axis is δ, the effective crossing angle $\delta_{\rm eff}$ between beam particles and photons depends on the spatial position of the interaction point with respect to the laser focus and can differ from δ by up to ξ, the laser focusing angle as defined in Eq. (99). The effective crossing angle $\delta_{\rm eff}$ needs to be calculated for each STE (primary and secondary) and α should be replaced by $\alpha_{\rm eff} = \pi + \delta_{\rm eff}$ in all formulas of Sec. 2.

Assume the average photon direction of propagation at the point (x'_0, y'_0, z'_0) in the laser CS is along $\vec{R}$, *i.e.* the tangent to the '$1/r$ envelope' of field intensity in the plane P defined by (x'_0, y'_0, z'_0) and the laser axis as shown in Fig. 14. The $1/r$ envelope is defined by the

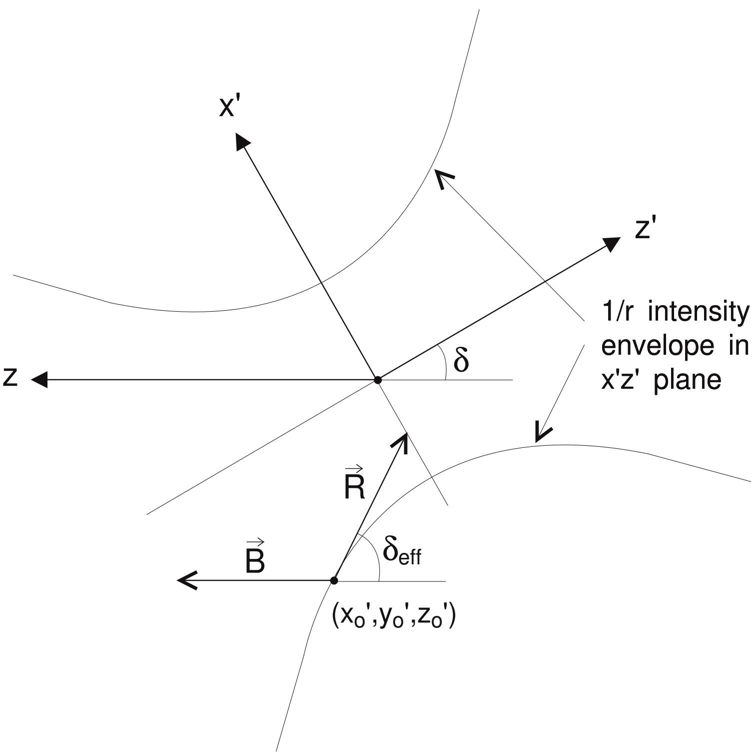

Figure 14: Crossing angle δ between the particle and laser beam axis and effective crossing angle δ_{eff} between laser photons propagating along $\vec{R}$ and beam particles moving along $\vec{B}$ at the interaction point (x'_0, y'_0, z'_0).

points (x', y', z') with

$$\rho_\omega(x', y', z') = \frac{1}{r} \cdot \rho_\omega(0, 0, z')\ , \tag{127}$$

where r is given by

$$r = \frac{\rho_\omega(x'_0, y'_0, z'_0)}{\rho_\omega(0, 0, z'_0)}\ . \tag{128}$$

In the plane P, the envelope is represented by the line

$$e(z') = \frac{\sqrt{x'^2_0 + y'^2_0}}{r(z'_0)} \cdot r(z'), \tag{129}$$

where $r(z')$ is the $1/e$ radius of field intensity as defined in Eq. (97).

Then, if $\vec{B}$ is a unit vector pointing along the beam, the effective crossing angle is given by

$$\tan \delta_{\mathrm{eff}} = -\frac{\left|\vec{B} \times \vec{R}\right|}{\vec{B} \cdot \vec{R}}\ , \tag{130}$$

with

$$\begin{aligned}
\left|\vec{B}\times\vec{R}\right| &= \sqrt{k^2 y_0'^2 + k^2 x_0'^2\cos^2\delta + z_0'^2\sin^2\delta + 2kx_0' z_0'\cos\delta\sin\delta}\ , && (131)\\
\vec{B}\cdot\vec{R} &= +kx_0'\sin\delta - z_0'\cos\delta \qquad \text{for } z_0' > 0\ ,\\
&= -kx_0'\sin\delta + z_0'\cos\delta \qquad \text{for } z_0' \le 0\ ,\\
k &= \frac{z_0'^2}{az_R^2 + z_0'^2}\ , && (132)
\end{aligned}$$

where z_R is the Rayleigh range (Eq. (95)) and a is the ratio of the effective and the diffraction limited focal spot area (Eq. (98)).

8.2 Effective Density of Beam Particles

Equation (103) gives the beam particle density $\rho_{\text{beam}}(x, y, z, t)$ assuming a three-dimensional Gaussian distribution. With this expression, ρ_{beam} can be calculated at the center of each STE. However, the beam particles have a path in the laser field before they reach the STE and are subject to interaction with laser photons. Some of the beam particles will be spent in these interactions and therefore the effective density $\rho_{\text{beam}}^{\text{eff}}$ of beam particles at the STE will be smaller than given by Eq. (103). The difference between ρ_{beam} and $\rho_{\text{beam}}^{\text{eff}}$ depends on the length and the field strength along the particle trajectory to the STE and can be substantial for very strong fields.

In the current version of NI, the calculation of the effective beam density is implemented only for an electron beam because of the following reasons:

1. All measurements at E-144 we done with an electron beam.
2. The probability for electrons to Compton scatter is orders of magnitude higher than for photons to convert into e^+e^- pairs, even in fields with $\Upsilon \sim 1$.
3. The total probability for Compton scattering can be approximated by the Klein-Nishina formula which allows a very efficient calculation of the effective density. No similar formula is available for the Breit-Wheeler or trident pair production.

Figure 15 shows how the correction to ρ_{beam} is obtained in NI. The STE is moved backwards in time through the laser field and the total interaction probability of electrons along this path is calculated with the Klein-Nishina approximation of Eq. (66). The step-size in this integration is given by Eq. (115), *i.e.* the same algorithm is used as in the integration over t' for secondary processes.

9 Speed Optimizations

One of the main goals of NI was to have a *fast* simulation tool, *i.e.* one that could provide results within a short time and for many different experimental conditions and processes. Therefore, execution speed was always a major concern in the program design.

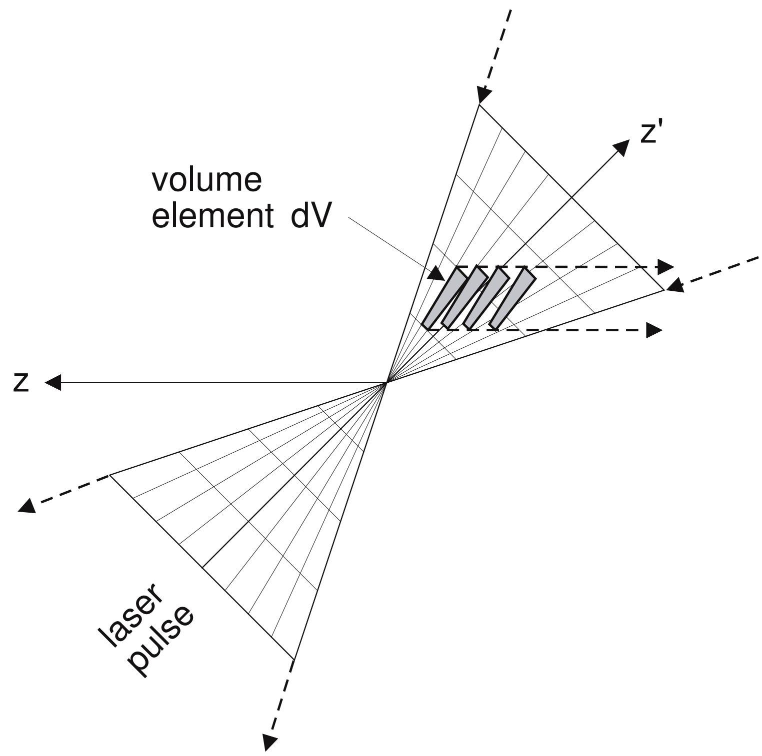

Figure 15: Procedure to calculate the effective density of beam particles. The STE is moved backwards in time out of the laser field and the total interaction probability of beam particles with the laser field along this path is calculated.

The speed optimization implemented in NI are guided by the following requirements and observations:

1. The experimentally observable particle spectra `phsp_nl[..]`, `elsp_nl[..]` and `posp_nl[..]` should be affected as little as possible.

2. Many STE have a low density of laser photons and beam particles and therefore contribute little to the total reaction rates.

3. Higher order processes are nonlinear in η^2 and their reaction yield is dominated by a few STEs with the highest field intensity.

4. Most CPU time is spent in calculating the secondary processes.

All speed optimizations are implemented as input parameters or program options and the level of optimization can be chosen by the user. Since the effect of these optimizations on the CPU time as well as on the results of specific processes or spectra can be substantial, it is important that the user is fully aware of these optimizations and understands what part of the calculation they affect.

With the speed optimization described below and the use of lookup tables as described in Sec. 10, the CPU time needed to simulate experimental conditions similar to E-144 became manageable. There is certainly more potential for further optimizations, but the programming time and especially the time needed for thorough testing of new code has to be taken into account as well.

9.1 Variable Step-Size in z' and Time

In Sec. 4 the integration over space and time was discussed, assuming a fixed step-size along the laser beam axis z' and in time t. However, this approach does not account for the rapid change in photon density close to the laser focus. Choosing a big step-size will result in a poor simulation of interactions close to the focal point (the most important part of the simulation). On the other hand, the small step-size necessary for an accurate simulation will be used throughout the simulation and will require a large amount of CPU time. A more efficient approach is to use a variable step-size in z' and t, larger for STEs far away from the focus and smaller for STEs close to the focus.

The algorithm implemented in NI uses the change in 'normalized photon density', *i.e.* $d\rho'$, as a criterion to adjust the step size. Ignoring the Gaussian profile of the laser pulse in z', *i.e.* assuming CW laser, the change in photon density along z' caused by the focusing is given by

$$\rho'(z') = \rho'_0 \cdot \frac{a \cdot A_0}{A(z')} = \rho'_0 \cdot \frac{a}{a + (z'/z_R)^2} \,, \tag{133}$$

where ρ'_0 is the normalized photon density at the focal point, a is the ratio of the effective (A_{eff}) and diffraction limited (A_0) focal spot size and $A(z')$ is the laser area as defined in Eq. (98). The distance $z'(k)$ from the focus for which

$$\rho'(z'(k)) \equiv (1 - k) \cdot \rho'_0 \,, \tag{134}$$

i.e. at which the normalized density $\rho'(z')$ has dropt by $1 - k$ with respect to ρ'_0, is given by

$$z'(k) = \pm z_R \cdot \sqrt{\frac{ak}{1-k}} \,. \tag{135}$$

The numeric integration NI takes the central values and step-sizes for z' and t from a fixed, precalculated grid of points $z'[i]$ along the z'-axis as shown in Fig. 16. This grid is centered at $z'[0] = 0$, *i.e.* the focal point, and the points close to the focus are determined by

$$z'[\pm i] = z'(i \cdot \Delta k), \tag{136}$$

where Δk is the maximum allowed change in normalized photon density between two points on the grid. Once the distance to the next point, *i.e.* $\Delta z'[i] = z'[i+1] - z'[i]$, evaluates to more than the default step-size dz' as defined in Eq. (107), the remaining points on the grid are equally spaced with distance dz'. Note that the integration range for both t and z' as discussed in Sec. 4 needs to be adjusted to coincide with points on the grid $z'[i]$.

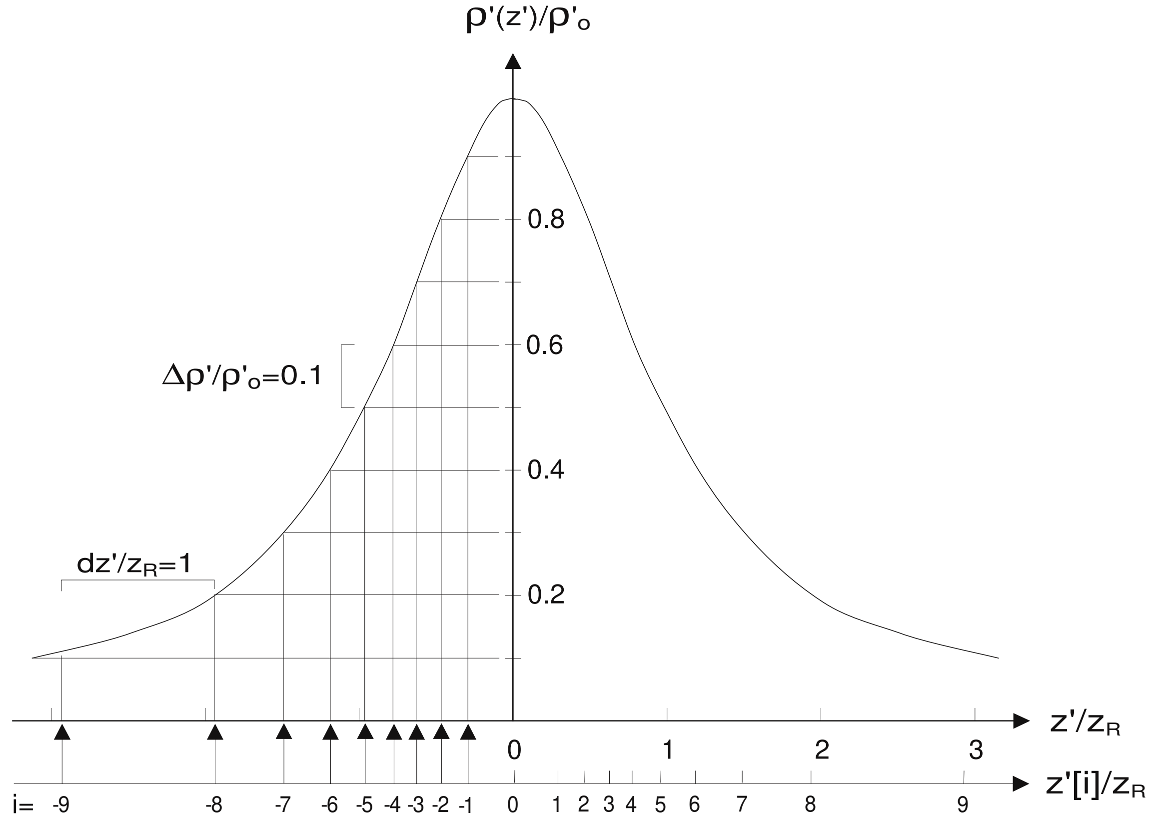

Figure 16: Example of a variable step-size grid for the integration in t and z', defined by the maximum change in normalized photon density $\Delta k = 0.1$ and a default step-size $dz' = z_R$.

9.2 Space-Time Elements with Low Reaction Yields

Many space-time elements in the integration have a low density both in laser photons and beam particles and their contribution to the total reaction yield is very small. The goal of the speed optimization discussed in this section is to avoid these primary STEs in the calculation.

The criterion implemented in NI to reject 'low yield' STEs is to test $P_{\rho\rho dV} = \rho_\omega \cdot \rho_{\mathrm{beam}} \cdot dV$, *i.e.* the product of the photon density, the beam particle density and the size of the volume element. This quantity is proportional to a linear interaction yield like $n = 1$ Compton scattering.

For a test of $P_{\rho\rho dV}$, the program first needs to calculate the maximum value $P^{\max}_{\rho\rho dV}$ for all primary STEs in the integration. Since arbitrary offsets in space $(x_{\mathrm{off}}, y_{\mathrm{off}})$ and time (t_{off}) between the two beams have to be taken into account, this calculation is not straightforward and the program needs to loop a first time over all STEs during the initialization phase in order to determine $P^{\max}_{\rho\rho dV}$. Then, in the actual integration, only STEs are considered with

$$P_{\rho\rho dV} \;>\; R_{\rho\rho dV} \cdot P^{\max}_{\rho\rho dV} \;, \tag{137}$$

where $R_{\rho\rho dV}$ is an input parameter to NI and represents the minimum ratio between $P_{\rho\rho dV}$ and $P^{\max}_{\rho\rho dV}$.

9.3 CPU Intensive, Nonlinear Processes

This speed optimization concentrates on the nonlinear dependence of higher order processes. This dependence implies that the reaction yield for such a process is more and more dominated by the contributions from a few STEs with the highest field intensities.

The procedure implemented in NI to optimize the calculation for higher order processes is very similar to the one discussed in the previous section 9.2. For each order n of an optimized process, the program compares the quantity $P_{\eta 2ndV} = \eta^{2n} \cdot dV$ with the maximum value $P^{\max}_{\eta 2ndV}$ for all primary STEs in the integration. Again, the maximum value $P^{\max}_{\eta 2ndV}$ is obtained by an explicit evaluation of the product $P_{\eta 2ndV}$ for all orders n and all STEs during the program initialization. Then, during the actual integration of an optimized process, only orders n are calculated for which

$$P_{\eta 2ndV} \; > \; R_{\eta 2ndV} \cdot P^{\max}_{\eta 2ndV} \; , \tag{138}$$

where $R_{\eta 2ndV}$ is a process specific input parameter to NI and represents the minimum ratio between $P_{\eta 2ndV}$ and $P^{\max}_{\eta 2ndV}$ for all orders n (*i.e.* one input parameter for each optimized process).

The optimization described above is intended for CPU intensive processes, *i.e.* mainly secondary processes, and the minimum ration $R_{\eta 2ndV}$ should be set to a small number, *e.g.* 10^{-4}. However, with the procedure as explained so far the following problem may arise. For very high orders n it is possible that only a single STE survives in the calculation, namely the STE that defines $P^{\max}_{\eta 2ndV}$. All other primary or secondary STEs with a slightly lower value of η are discarded. For example, assuming that dV is fixed and η is still 90% of the maximum value, the ratio $P_{\eta 2ndV}/P^{\max}_{\eta 2ndV}$ for order $n = 100$ is already as low as 7×10^{-10}.

To limit the calculation of very high orders to a single STE may be an optimization too drastic and can be softened by a procedure that considers the following additional criterion. The program also calculates the product $P_{\eta 2dV} = \eta^2 \cdot dV$ and compares it to the maximum value $P^{\max}_{\eta 2dV}$. The ratio $P_{\eta 2dV}/P^{\max}_{\eta 2dV}$ is required to exceed the minimum value $R_{\eta 2dV}$, *i.e.*

$$P_{\eta 2dV} > R_{\eta 2dV} \cdot P^{\max}_{\eta 2dV} \; . \tag{139}$$

$R_{\eta 2dV}$ is an additional process specific input parameter to NI and should be set to a value of order 0.5. Then, all orders n in a STE are included in the calculation if at least one of the two criteria is satisfied. For low orders, $R_{\eta 2ndV}$ selects the STE to be considered, but for high orders it is $R_{\eta 2dV}$.

In the current version of NI, this type of optimization is implemented for secondary nonlinear Compton scattering (P2_NLCS), secondary multiphoton Breit-Wheeler pair production (P2_BW) and both primary and secondary multiphoton trident pair production (P1_WWBW and P2_WWBW).

9.4 Optimizing Secondary Compton Scattering

The optimizations discussed in this section are intended to make the calculation of *secondary* nonlinear Compton scattering more efficient. They are based on the strongly nonlinear dependence of high order processes on the field intensity as well as the shape of the energy spectra for these high order interactions. Note that the simulation of the primary processes are not affected by these program options.

9.4.1 Cutoff in Electron Spectrum

For field intensities of $\eta^2 \ll 1$, secondary Compton scattering is only important in areas where a secondary process of lower order can compete with a primary process of higher order, *e.g.* the electron spectrum below the linear Compton edge can have comparable contributions from double $n = 1$ scattering and single $n = 2$ scattering. However, for electron energies above the linear Compton edge, the spectrum is completely dominated by primary $n = 1$ Compton scattering because no secondary process of lower order exists. Therefore, ignoring secondary Compton scattering for interactions where the scattered electron energy is above a cutoff E'_{max}, has a small effect on the total electron and photon spectra. In addition, the photon spectrum is affected only at the low energy part which has little importance in further Breit-Wheeler pair productions.

Of course, this cutoff in energy could just as well be implemented as a minimum energy for the scattered photon. However, in experiment E-144 it was primarily the electron spectrum that was measured and a cutoff in the experimentally observed spectrum seemed natural. In most of these measurements, the momentum range of the electron calorimeter (ECAL) was limited to the region below the linear Compton edge and a simulation of this specific experimental setup would justify a cutoff energy even for $\eta^2 \sim 1$.

Note that for general (*i.e.* not detector specific) simulations, this optimization should be used only for $\eta^2_{\text{max}} < 1$ and $E'_{\text{max}} > E_{\text{beam}} - \omega'_{\text{max}}(1)$, *i.e.* the cutoff energy should be above the linear Compton edge in the electron spectrum.

9.4.2 Reduced Energy Range for Higher Orders

The size and shape of the photon energy spectrum for NLCS of order n in field with intensity η is sketched in Fig. 17 and can be characterized as follows:

1. The yield is suppressed by order $1/\eta^2$ with respect to the spectrum for order $n - 1$.
2. The spectrum extends beyond the spectrum for order $n-1$, *i.e.* $\omega'_{\text{max}}(n) > \omega'_{\text{max}}(n-1)$.
3. The spectrum peaks close to the endpoint $\omega'_{\text{max}}(n)$.

This suggests to limit the integration range of the scattered photon energy ω' for order n processes to values for which this order is dominant, namely the region where the spectrum extends beyond the previous order.

The algorithm implemented in NI to adjust the lower integration limit $\omega'_{\text{min}}(n)$ of the photon energy for NLCS of order n takes into account the field intensity η and calculates

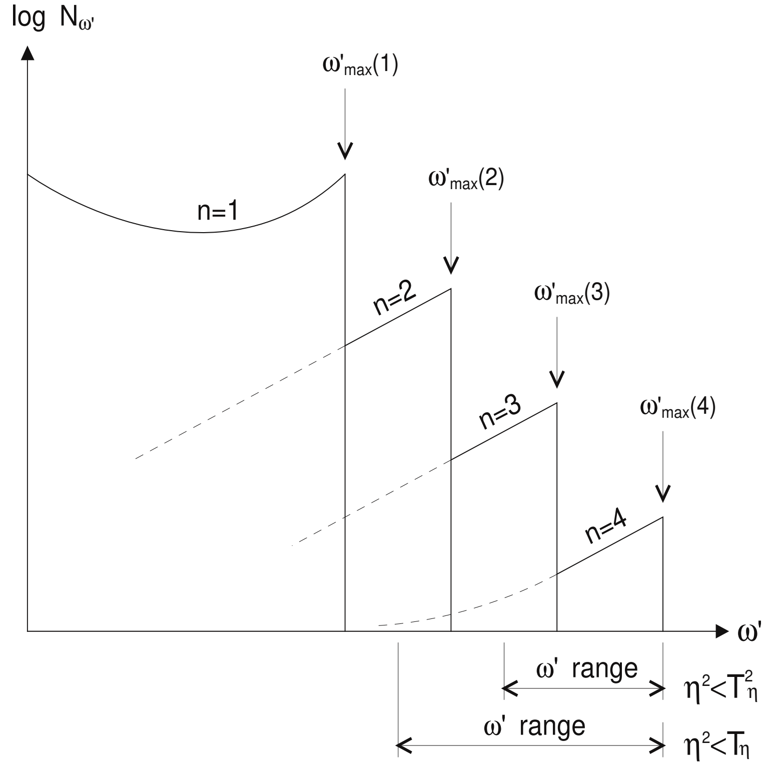

Figure 17: Reduced integration range in the scattered photon energy ω' for secondary NLCS of order n=4. The lower boundary depends on the field intensity and is $(\omega'_{\max}(2)+\omega'_{\max}(3))/2$ for $\eta^2 < T^2_{\eta 2}$ and $(\omega'_{\max}(1)+\omega'_{\max}(2))/2$ for $\eta^2 < T_{\eta 2}$.

$\omega'_{\min}$ for each secondary STE and order n according to

$$\eta^2 \leq T^2_{\eta 2}: \quad \omega'_{\min}(n) = \frac{\omega'_{\max}(n-2)+\omega'_{\max}(n-1)}{2} \qquad \text{for } n > 2\,, \tag{140}$$

$$= 0.95 \cdot \omega'_{\max}(1) \qquad \text{for } n = 2\,, \tag{141}$$

$$= 0 \qquad \text{for } n = 1;\,, \tag{142}$$

$$\eta^2 \leq T_{\eta 2}: \quad \omega'_{\min}(n) = \frac{\omega'_{\max}(n-3)+\omega'_{\max}(n-2)}{2} \qquad \text{for } n > 3\,, \tag{143}$$

$$= 0.95 \cdot \omega'_{\max}(1) \qquad \text{for } n = 3\,, \tag{144}$$

$$= 0 \qquad \text{for } n \leq 2\,, \tag{145}$$

where $T_{\eta 2}$ is an input parameter to NI and $T^2_{\eta 2}$ is approximately the size of the error introduced by this optimization.

9.5 Optimizing Breit-Wheeler Pair Production

The energy spectra (in the LAB frame) of electrons and positrons produced in multiphoton Breit-Wheeler processes are basically symmetric to half the energy of the initial high-energy photon for all orders n of the process and only the widths of these distributions depend on n. Therefore, in an experiment like E-144 where the positron spectrum is measured, it is hard to distinguish the different orders of the process. This is distinct from the situation in nonlinear Compton scattering where the shape and range of the spectra are characteristic of the process order n. This motivates to limit the calculation of the primary and secondary Breit-Wheeler pair production to orders n with a significant contribution to the total yield of e^+e^- pairs.

As shown in Fig. 12, the program loops over the process orders n for each energy bin of the input photon spectrum at each primary and secondary STE. The optimization implemented in NI keeps track of $W_{e^+e^-}(n)$, *i.e.* the contribution of order n, and terminates the loop as soon as

$$W_{e^+e^-}(n) < W^{\max}_{e^+e^-} * R_{\mathrm{BW}} \, , \tag{146}$$

i.e. the contribution $W_{e^+e^-}(n)$ of the last calculated order has dropped below the fraction R_{BW} with respect to the maximum contribution $W^{\max}_{e^+e^-}$ of all orders calculated so far. The minimum ratio R_{BW} is an input parameter to NI.

Note that, based on the same arguments, this optimization could also be implemented for the multiphoton trident pair production, primary and secondary. However, because of the reasons mentioned above as well as the sensitivity of the Breit-Wheeler pair production on the higher order contributions of NLCS to the photon spectrum, this procedure should not be applied to Compton scattering.

9.6 Effect of Optimizations

Figure 18 shows the effect the speed optimizations described above have on the precision and the speed of the simulation at the example of a primary electron beam colliding with a circularly polarized, green laser. The processes considered for this test are P1_NLCS, P1_WWBW, P2_NLCS and P2_BW up to order $n = 20$ and the laser pulse, electron beam and space-time grid are defined by typical parameters. Excluded from this comparison is the gain in simulation efficiency obtained by a variable step-size in z' and time as described in Sec. 9.1. As mentioned earlier, this optimization achieves a higher precision result with little cost in CPU time and was active for all test calculations described below with a parameter value of $\Delta k = 0.2$.

The following set of results are chosen to monitor the impact of the various optimizations on the precision of the simulation:

- N_{ph}, all: the total number of photons produced in the collision,
- N_{e+e-}, all: the total number of e^+e^- pairs produced in the collision,
- N_{e+e-}, trid: the number of e^+e^- pairs produced by multiphoton trident (WWBW) pair production,

	Speed Optimizations					
	none	$R_{\rho\rho dV}$ $=10^{-2}$	$\oplus$ $R_{\eta 2ndV}$ $=10^{-3}$ ¦ $R_{\eta 2dV}$ $=0.6$	$\oplus$ E'_{max} $=20$	$\oplus$ $T_{\eta 2}$ $=0.1$	$\oplus$ R_{BW} $=10^{-3}$
N_{ph}, all	$2.25\text{x}10^{7}$	95.6 %	95.6 %	94.7 %	94.7 %	94.7 %
N_{e+e-}, all	$4.66\text{x}10^{-2}$	99.8 %	98.6 %	98.6 %	98.6 %	98.6 %
N_{e+e-}, trid	$2.47\text{x}10^{-5}$	100 %	96.9 %	96.9 %	96.9 %	96.9 %
N_{e-}, n=1 (19-20 GeV)	$1.09\text{x}10^{6}$	95.7 %	95.7 %	95.7 %	95.7 %	95.7 %
N_{e-}, n=2 (14-15 GeV)	$3.59\text{x}10^{4}$	99.4 %	99.3 %	99.0 %	99.0 %	99.0 %
N_{e-}, n=3 (9-10 GeV)	$1.41\text{x}10^{3}$	99.7 %	99.6 %	99.5 %	99.4 %	99.4 %
N_{e-}, n=4 (6-7 GeV)	$1.22\text{x}10^{1}$	99.8 %	99.6 %	99.5 %	99.2 %	99.2 %
calls to NLCS	$2162\text{x}10^{6}$	29.1 %	3.81 %	2.14 %	1.23 %	1.23 %
calls to MPBW	$483\text{x}10^{6}$	53.7 %	4.05 %	4.05 %	4.05 %	2.25 %
calls to WWBW	$131\text{x}10^{6}$	23.6 %	0.63 %	0.63 %	0.63 %	0.63 %
total calls	$2775\text{x}10^{6}$	33.1 %	3.70 %	2.40 %	1.69 %	1.38 %
total CPU (SLAC sec)	25742	30.7 %	3.77 %	2.49 %	1.80 %	1.56 %

Figure 18: Impact of the various speed optimization on the precision and execution speed of the simulation. The vertical columns show the combined effect (indicated by the $\oplus$ sign) of the optimization listed at the top and to the left of the column. The first column labeled 'none' includes no optimizations and lists the actual values of the 'precision' and 'speed' monitors. All other columns show the fraction of these monitor values with respect to the first column. The combined effect of all optimizations on the simulation results is less than 5.5% while the execution speed is increased by a factor of ~ 65.

- N_{e-}, n=1, 19-20 GeV: the number of electrons with energy between 19 and 20 GeV, produced in large part by $n = 1$ Compton scattering,
- N_{e-}, n=2, 14-15 GeV: the number of electrons with energy between 14 and 15 GeV, produced in large part by $n = 2$ Compton scattering,
- N_{e-}, n=3, 9-10 GeV: the number of electrons with energy between 9 and 10 GeV, produced in large part by $n = 3$ Compton scattering,
- N_{e-}, n=4, 6-7 GeV: the number of electrons with energy between 6 and 7 GeV, produced in large part by $n = 4$ Compton scattering.

The number of calls to basic differential reaction rate routines and the total CPU time needed for the simulation are used to measure the effect of the optimizations on the execution speed:

- calls to NLCS: the number of calls to the basic NLCS routine,
- calls to MPBW: the number of calls to the basic MPBW routine,
- calls to WWBW the number of calls to the basic WWBW routine,
- total calls: the total number of calls to basic differential reaction rate routines,
- total CPU: the total CPU time needed for the simulation in normalized SLAC CPU seconds.

The table in Fig. 18 shows in the first column the actual values of the 'precision' and 'speed' monitors described above for a simulation with none of the optimizations active. The second column lists the fraction of these monitor values with respect to the first column when one of the speed optimization is turned on, namely rejecting STEs with a low reaction yield and a parameter value of $R_{\rho\rho dV} = 10^{-2}$. The third column shows the combined effect (indicated by the $\oplus$ sign) of the first optimization and the optimization for CPU intensive, nonlinear processes with parameters $R_{\eta 2ndV} = 10^{-3}$ and $R_{\eta 2dV} = 0.6$ for the processes P1_WWBW, P2_NLCS and P2_BW. In the remaining columns, the three optimizations for P2_NLCS are made active one by one.

In summary, the combined effect of all optimizations on the precision of the result is in the worst case ~ 5 % while the gain in execution speed is a factor of ~ 65. Of course, these numbers depend on the type of simulation and the values chosen for the optimization parameters.

10 Lookup Tables for Bessel- and A_i-Functions

The most dramatic gain in execution speed is achieved by using lookup tables (LTs) to store the values of the Bessel-functions $J_n(z)$ and the functions $A_i(n, a, b)$ which are needed to calculate the differential reaction rates of Sec. 2. Each order n of a function is represented by one or more LTs.

The LTs are one-dimensional ($J_n(z)$) or two-dimensional ($A_i(n, a, b)$) arrays in memory. The elements of such an array store the values of the function for a discrete set of function arguments. In the actual integration, the function value for a specific argument is approximated by a linear interpolation in one or two dimensions between values stored in the LT for the arguments nearest the specific argument.

In the current version of NI the LTs are recalculated each time the program runs. Another approach would be to read the elements of the LTs from an external file. However, the CPU time spent in calculating the LTs is usually a small fraction of the time needed for the simulation. Furthermore, the range of function arguments a LT needs to cover depends on various input parameters of NI.

10.1 Bessel-Functions

All LTs for the Bessel-functions have equal dimensions D_z^{LT}, independent of the interaction order n they represent, and store values at equally spaced arguments $z_n[i]$ defined as

$$z_n[i] \equiv i \cdot \frac{z_{\max}(n)}{D_z^{LT} - 1} , \qquad i = 0 \ldots D_z^{LT} - 1 . \tag{147}$$

The upper limit of the argument z to the Bessel-functions for an interaction of order n is given by

$$z_{\max}(n) = \frac{n\eta_{\max}}{\sqrt{1 + \eta_{\max}^2}} , \tag{148}$$

where $\eta_{\max}$ is the maximum value of η for all STEs.

Two groups of LTs are supported for the Bessel-functions. The first group is defined by

$$LT_{J2}^n[i] \equiv J_n^2(z_n[i]) \tag{149}$$

and consists of $O_{\max} + 2$ lookup tables (*i.e.* $n = 0 \ldots O_{\max} + 1$), where $O_{\max}$ is the maximum order n of a nonlinear process considered in the simulation. Note that an evaluation of a differential reaction rate requires three calls to LTs in this group, *i.e.* LT_{J2}^{n-1}, LT_{J2}^n and LT_{J2}^{n+1}.

The second group has two LTs for each order n of interaction and they are defined as

$$LT_{J2}^n[i] \equiv J_n^2(z_n[i]) , \tag{150}$$

$$LT_{J2S}^n[i] \equiv J_{n-1}^2(z_n[i]) + J_{n+1}^2(z_n[i]) - 2J_n^2(z_n[i]) . \tag{151}$$

This group needs almost twice as much memory as the first group to store LTs, but a differential reaction rate can be calculated with only two calls to LTs. The second group allows for a higher execution speed of NI and should be used unless memory limitations are an issue.

10.2 A_i-Functions

All LTs for the A_i-functions have equal dimensions D_a^{LT} for the argument a and D_b^{LT} for the argument b, independent of the interaction order n they represent. They store values at equally spaced arguments $a_n[i]$ and $b_n[j]$ defined as

$$a_n[i] \equiv a_{\min}(n) + i \cdot \frac{a_{\max}(n) - a_{\min}(n)}{D_a^{LT} - 1}, \qquad i = 0 \ldots D_a^{LT} - 1, \tag{152}$$

$$b_n[j] \equiv b_{\min}(n) + j \cdot \frac{b_{\max}(n) - b_{\min}(n)}{D_b^{LT} - 1}, \qquad j = 0 \ldots D_b^{LT} - 1. \tag{153}$$

The lower and upper limits of the arguments a and b to the A_i-functions for an interaction of order n is given by

$$a_{\min} = 0, \tag{154}$$

$$a_{\max} = \frac{\sqrt{2}\, n_{\max}\, \eta_{\max}}{\sqrt{1+\eta_{\max}^2}}, \tag{155}$$

$$b_{\min} = -\frac{n_{\max}}{2} \cdot \frac{\eta_{\max}^2}{\sqrt{1+\eta_{\max}^2}}, \tag{156}$$

$$b_{\max} = -b_{\min}, \tag{157}$$

where $\eta_{\max}$ is the maximum value of η for all STEs and $n_{\max}$ is either n or $n+2$ depending on the group of LTs (see below). Note that the lower limit of a is zero because the integration range of ϕ is $[0, \pi/2]$ and therefore $a \equiv a' \cdot \cos\phi$ is in the range $[0, a'_{\max}]$ with $a'_{\max} = a_{\max}$. Also note that for simulations that consider only NLCS processes (and no MPBW or WWBW pair production) the maximum value of b is zero.

Again two groups of LTs are supported. The first group is a minimal solution that requires little memory to store the LTs, but also does not take full advantage of the potential to increase the execution speed. For this group, $n_{\max} = n+2$ and the LTs are defined as

$$LT_{A0}^n[i,j] \equiv A_0(n, a[i], b[j]). \tag{158}$$

This first group consists of $O_{\max}+4$ lookup tables (*i.e.* $n = -1 \ldots O_{\max}+2$), where $O_{\max}$ is the maximum order n of a nonlinear process considered in the simulation. The evaluation of a differential reaction rate requires five calls to LTs for each step in the ϕ-integration, *i.e.* $LT_{A0}^{n\pm 2}$, $LT_{A0}^{n\pm 1}$ and LT_{A0}^{n}. Then, relations (8) and (9) are used to calculate $A_1(n,a,b)$ and $A_2(n,a,b)$.

A fundamental difference between the differential reaction rates for a circularly and a linearly polarized laser field is the additional integration over ϕ in the latter case. Therefore, if LTs of the first group are used in the simulation, this additional integration will approximately increase the CPU time needed by a factor of N_ϕ, *i.e.* the number of steps in the ϕ-integration, compared to an equivalent simulation with a circularly polarized laser. However, the LTs can be chosen such that they include the integration over ϕ, *i.e.*

$$LT_{A02}^n[i,j] \equiv \int_0^{\pi/2} d\phi A_0^2(n, a'[i]\cos\phi, b[j]), \tag{159}$$

$$LT^n_{SA}[i,j] \equiv \int_0^{\pi/2} d\phi \left\{ A_1^2(n, a'[i]\cos\phi, b[j]) - A_0(n, a'[i]\cos\phi, b[j]) A_2(n, a'[i]\cos\phi, b[j]) \right\} , \quad (160)$$

$$LT^n_{\sigma' A02}[i,j] \equiv \int_0^{\pi/2} d\phi \sigma'(n, a'[i]\cos\phi, b[j]) \cdot A_0^2(n, a'[i]\cos\phi, b[j]) , \quad (161)$$

where $a'[i]$ is defined by $a[i] \equiv a'[i]\cos\phi$. With these LTs, the computational effort for a simulation of a linearly polarized laser is comparable to that of a circularly polarized laser. This group consists of $3 \cdot O_{\rm max}$ lookup tables and the value of $n_{\rm max}$ is n. Only three calls to LTs are required in order to evaluate a differential reaction rate. Note that the third type of LTs in this group, *i.e.* $LT^n_{\sigma' A02}$, is needed only if polarization effects in the backscattered photon beam are taken into account.

Of course, the calculation of the ϕ-integrated LTs can by itself require a considerable amount of CPU time. In order to speed up this calculation, the program first builds the temporary LTs

$$T^n_{A02}[i,j] \equiv A_0^2(n, a[i], b[j]) , \quad (162)$$

$$T^n_{SA}[i,j] \equiv A_1^2(n, a[i], b[j]) - A_0(n, a[i], b[j]) A_2(n, a[i], b[j]) , \quad (163)$$

which are then used to perform the integration over ϕ. The dimensions of the temporary LTs in a and b can optionally be increased.

11 Installing and Running the Numeric Integration Program

Figure 19 shows the files needed to run the numeric integration program as well as the output files produced by NI. From the include (`*.h`) and program (`*.c`) files, the compiler and linker generates the executable image `ni.exe` (or `ni` under UNIX). The input parameters for the simulation are read by the executable image from the file `<ni>.inp` during program execution. The simulation results are saved in the 'log-file' `<ni>.log`, the histogram-file `<ni>.his` and optionally in the lookup-table files `<nilt>.asc` and `<nilt>.bin`.

11.1 Program and Input Files

The program and input files specific to the numeric integration are described in some detail below. The 'general E-144 files' are used also by the E-144 data acquisition and analysis software and other E-144 programs and are not described here.

`ni.c`

is the 'main' program file, *i.e.* it contains the routine `main()`. This file serves as a user interface to the basic numeric integration routines `init_ni()`, `do_ni()` and `end_ni()` which reside in `nilib.c`. The default action of `ni.c` is to perform a single simulation for the

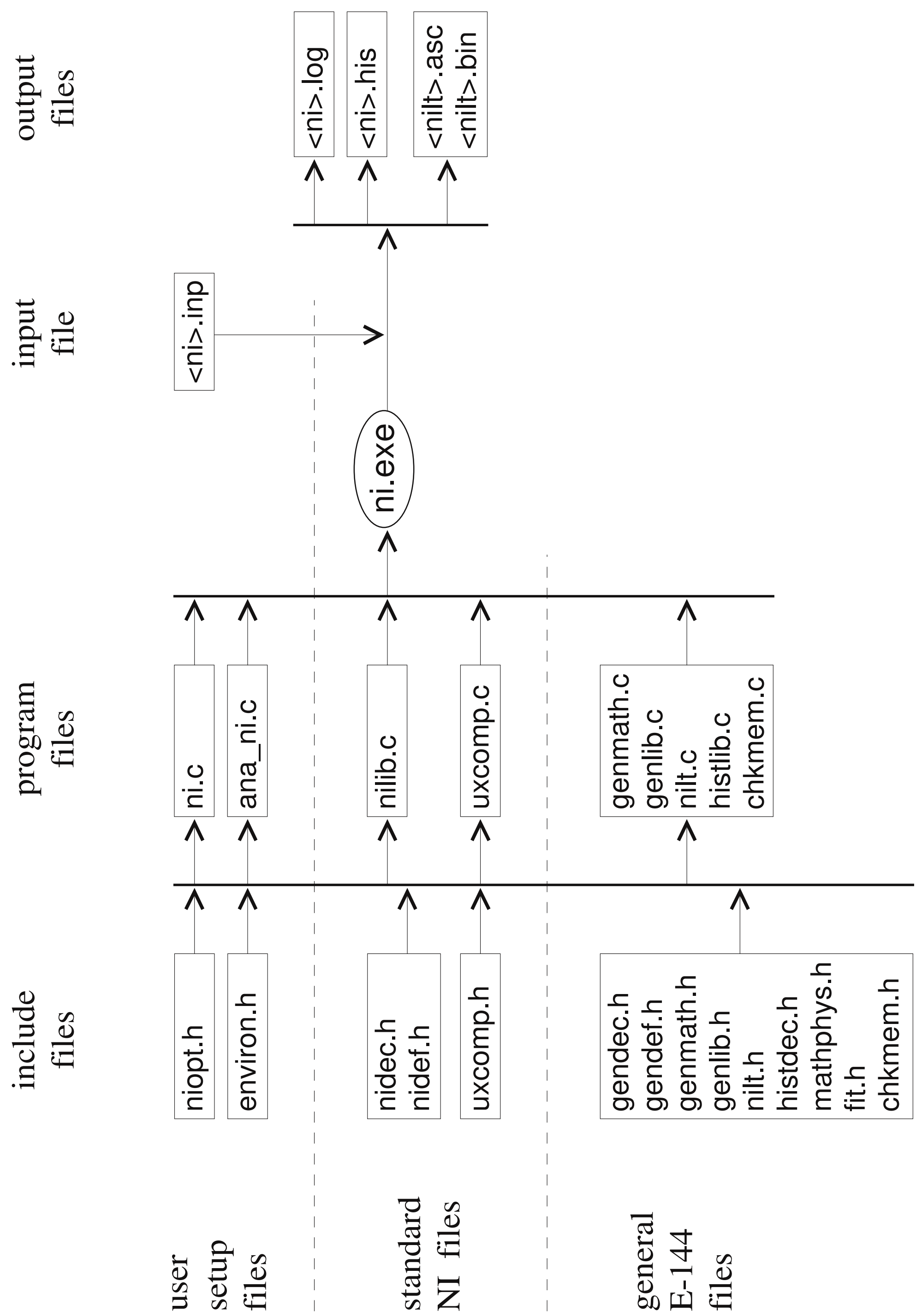

Figure 19: Source, input and output files of the numeric integration program.

parameters specified in `<ni>.inp`. As an illustration of how to perform multiple simulations in a single program run, the file also contains the routine `do_multi_event()` and an example of how to call it. Of course, the user is free to set up more sophisticated interface routines to simulate many experimental situations in a single program run.

Two additional routines, *i.e.* `step_parameter_linear()` and `step_parameter_log()` are provided to generate numeric integration lookup tables (NILTs) that store the results of many simulations in a standard format and can be read by the E-144 analysis software and other utility programs [10]. These routines perform multiple simulations while varying a single input parameter within a specified range. One of the two routines is called automatically if the following command-line arguments are provided with `ni.exe`:

```
ni  <rn> <fi> <fo> <mo> <lb> <ub> <np>
```

where

`<rn>` = run-number or parameter type, *i.e.*
1=peak η, 2=laser focal area $A_{\rm eff}$, 3=laser pulse width $\tau_{\rm laser}$,
4=beam σ_x, 5=beam σ_y, 6=beam pulse width $\tau_{\rm beam}$,
7=offset in time ($t_{\rm off}$), 8=offset in x ($x_{\rm off}$), 9=offset in y ($y_{\rm off}$),
`<fi>` = body of intput file name (without path and extension),
`<fo>` = body of output file names (without path and extensions),
`<mo>` = step-mode, either 'lin' or 'log', *i.e.*
'lin' = equidistant steps on linear scale,
'log' = equidistand steps on logarithmic scale,
`<lb>` = lower boundary of parameter range,
`<ub>` = upper boundary of parameter range,
`<np>` = number of points in parameter range (including `<lb>` and `<ub>`).

`ana_ni.c`

is the user analysis file and contains the analysis entry points described in Sec. 6. The routines provided by `ana_ni.c` are:

`init_analyse()`	initialize the analysis, *i.e.* book the histograms,
`end_analyse()`	final call to analysis, *e.g.* normalize histograms,
`analyse_stp()`	analysis of primary STE (before and after secondary processes),
`analyse_stp_p2()`	analysis of secondary STE, *i.e.* STE of secondary processes,
`analyse_loop()`	'innerst loop' analysis.

Many histograms are already defined in `ana_ni.c` and groups of these histograms can easily be selected by program parameters close to the top of the file. However, this file is considered to be user specific and the user should feel free to add whatever histograms he needs to his own copy of `ana_ni.c`.

`nilib.c`

is the numeric integration library and contains all routines necessary for the simulation. This file is not a user file and should only be changed for further program development. The program initialization is done in `init_ni()`, the actual simulation is performed by calling `do_ni()` and program termination is handled by `end_ni()`. Each physics process is represented by a main routine, *e.g.* `do_nlcs()` for nonlinear Compton scattering. These main process routines are called by two interface routines for primary and secondary interactions, *e.g.* `do_p1_nlcs()` and `do_p2_nlcs()`, which themselves are call for each STE by `do_ni()`. In addition, `nilib.c` contains a large number of routines to handle all other calculations needed for the simulation, *e.g.*

`get_start_stop()`:	find t_{start} and t_{stop} for the time integration (Sec. 4),
`get_zstep()`:	calculate the grid $z'[i]$ for variable step-sizes along the laser beam axis z' and time t (Sec. 9.1),
`get_eta2n_dv_peak()`:	find the peak value of $\rho_\omega \cdot \rho_{\mathrm{beam}} \cdot dV$ and $\eta^{2n} \cdot dV$ for all primary STE (Sec. 9.2),
`getphi()`:	calculate the effective crossing angle δ_{eff} for the current STE (Sec. 8.1),
`get_el_rho_eff()`:	calculate the effective electron density for the current STE (Sec. 8.2),
`build_xxx_table()`:	build the LTs of type `xxx` (Sec. 10),
`lookup_xd()`:	lookup a function value in a LT of dimension $\mathtt{x} = 1$ or 2.

nidec.h, nidef.h

contain the definitions of preprocessor parameters, program variables and arrays as well as function declarations. This file is not a user file and should only be changed for further program development.

niopt.h

contains the program parameters implemented as preprocessor directives and parameters. This file needs to be set up prior to compiling and linking the program as explained in detail in Sec. 11.3.

environ.h

specifies the program environment, *i.e.* the operating system and the path to the program files. This file needs to be set up only when the software is originally installed on a new machine or in a new directory (see Sec. 11.5).

<ni>.inp

contains the program input parameters and is read by the executable image `ni.exe` during program execution. This file needs to be set up prior to running the program as explained in detail in Sec. 11.4.

uxcomp.c, uxcomp.h

are needed to run the program under the UNIX or LINUX operating systems and provide replacement routines for Microsoft C/C++ specific library functions.

chkmem.c, chkmem.h

are needed to run the program under the DOS operating system and contain a collection of memory diagnostic routines (useful for adjusting stack size and debugging 'memory leaks').

11.2 Output Files

<ni>.log

is the 'log-file' of the program and contains

- all error and warning messages generated during program execution,
- a detailed description of all program options and input parameters,
- a detailed description of many additional parameters calculated for the laser beam, the electron beam and the grid in space and time,
- the CPU time needed for the complete simulation and for each step in time,
- the final energy spectra of photons, electrons, positrons and e^+e^- pairs,
- the interaction yield as a function of process order n, *i.e.* the number of laser photons absorbed in the interaction, for each selected process.

An (shortened) example of a 'log-file' is listed below:

```
INF: --> Build LT for A0^2, A1^2-A0A2 (and Sigma*A0^2), n=1
INF:     (INT: 79600 (0.997) S_1:     0 (0.000) S_2:   200 (0.003) FAIL:     0 (0.000))
    <... more similar lines here ...>
INF: --> Build LT for A0^2, A1^2-A0A2 (and Sigma*A0^2), n=8
INF:     (INT: 79720 (0.999) S_1:    39 (0.000) S_2:    41 (0.001) FAIL:     0 (0.000))
INF:
INF: ==> This is log-file /home/bula/numint/log/doc_exa.log
INF:
INF: ******************************
INF: START OF NUMERICAL INTEGRATION
INF: ******************************
INF:
INF: Program Options:
INF: ----------------
INF: EL_BEAM: Primary Beam: Monochromatic Electron Beam
INF: LINEAR_POL: Linearly Polarized Laser
INF: NSTEP_NU:      Nr of Steps in Nu -Int (default)     : 60
INF: NSTEP_CYCLE:   Min Nr of Steps per Order n in Nu-Int: 6
INF: NSTEP_PHI:     Nr of Steps in Phi-Integration       : 30
INF: AIFCT_ERR_N:   Max Error in Ai-Fct per Order n      :    1.000E-02
INF: MAX_AIFCT_ERR: Upper limit of n*AIFCT_ERR_N         :    5.000E-01
INF: USE_A02_TABLE: LT for A02, A12-A0A, 200x200 values, double
INF: TLT_DIMF_A:    -->  A-dim of temp LT increased by 2
INF: TLT_DIMF_B:    -->  B-dim of temp LT increased by 1
INF: INTERPOLATE_LOOKUP_TABLE: interpolate values in lookup-tables
INF: USE_FOCUS_ANGLE: take into account laser focus angle
```

```
INF: USE_ELECTRON_SPENDING: take into account electron spending
INF: USE_GAMMA_POLARIZATION: take into account gamma beam polarization
INF:   -> USE_ENEDEP_GP: use energy-dependent polarization
INF: (MIN_)MAX_PHOTON_NLCS: Orders of n for Compton Scatt: 1 to 8
INF: (MIN_)MAX_PHOTON_BW:   Orders of n for Breit-Wheeler: 1 to 8
INF:
INF: Considered Processes:
INF: ---------------------
INF: PRIMARY  : P1_NLCS:  Non-Linear Compton Scattering
INF: PRIMARY  : P1_WWBW:  Multi-Photon Breit-Wheeler with WW Gamma Spectrum
INF: PRIMARY  : P1_NLCS_TOT: Fast Approx of Total n=1,2 Rate for NLCS
INF: SECONDARY: P2_NLCS:  Non-Linear Compton Scattering
INF: SECONDARY: P2_BW:    Multi-Photon Breit-Wheeler
INF:
INF: Speed Optimizations:
INF: --------------------
INF: *** Minimum ratios (eta^2n*dV)/(eta^2n*dV)_peak for order n:
INF:   - P2_NLCS:  E2NDV_MF_P2_NLCS:    1.000E-03
INF:   - P2_BW:    E2NDV_MF_P2_BW:      1.000E-03
INF:   - P1_WWBW:  E2NDV_MF_P1_WWBW:    1.000E-03
INF:
INF: *** Minimum ratios (eta^2*dV)/(eta^2*dV)_peak for any order:
INF:   - P2_NLCS:  E2DV_MF_P2_NLCS:     6.000E-01
INF:   - P2_BW:    E2DV_MF_P2_BW:       6.000E-01
INF:   - P1_WWBW:  E2DV_MF_P1_WWBW:     6.000E-01
INF:
INF: P2_NLCS : ELSP_CUTOFF:      skip process for final Ee-  >  20.00 [GeV]
INF: P2_NLCS : ETA2_THRESHOLD:   reduced gamma spec if eta2  <  0.100
INF: P1(2)_BW: N_BW_CUTOFF:      stop n-loop if yi(n)/yi_max <    1.000E-03
INF:
INF: Primary Space-Time Point Analysis:
INF: ---------------------------------
INF: ANA_NL_QED_STP: Non-Linear QED Processes
INF:
INF: Input Parameters for Laser:
INF: ---------------------------
INF: Wavelength of Laser Photons :        0.527 [um]
INF: Ratio A_eff(0)/A_diff_limit :        4.000
INF: Ratio Sigma(x)/Sigma(y)     :        1.000
INF: Crossing Angle (Laser,-Beam):       17.000 [Deg]
INF: Energy of Laser Pulse       :        0.400 [Joule]
INF: f-Number of focusing optics :        6.000
INF: FWHM(t) of Laser Intensity  :        1.500 [psec]
INF: Delay of Laser wrt Beam     :        0.000 [psec]
INF: X-Offset of Laser wrt Beam  :        0.000 [um]
INF: Y-Offset of Laser wrt Beam  :        0.000 [um]
INF:
INF: Input Parameters for Electron Beam:
INF: ----------------------------------
INF: Energy of Electrons         :       46.600 [GeV]
INF: Nr of Electrons in Bunch    :    1.000E+10
INF: Sigma(x) of Electron Density:       25.000 [um]
INF: Sigma(y) of Electron Density:       25.000 [um]
INF: FWHM(t)  of Electron Density:        5.000 [psec]
INF:
INF: Input Parameters for Space-Time-Energy Lattice:
INF: ----------------------------------------------
INF: Spatial Range in xp         :        3.000 [Sigmas]
INF: Spatial Range in yp         :        3.000 [Sigmas]
INF: Spatial Range in zp         :        3.000 [Sigmas]
INF: Nr of Steps in xp           :            9
INF: Nr of Steps in yp           :            9
INF: Nr of Steps in zp           :            9
INF: Pho Dens Step-Size at Focus :        0.200
```

```
INF: Delta(z0)/Delta(zp)         :        1.000
INF: Min Frac of Rho*Rho*DV Peak :    1.000E-02
INF: Min Frac of Eta^2*DV  Peak  :        0.001
INF: Maximum Energy              :       50.000
INF: Energy Bin-Width            :        1.000
INF:
INF: Calculated Laser Parameters:
INF: ---------------------------
INF: Energy of Laser Photons     :        2.353  [eV]
INF: Total Nr of Photons         :    1.061E+18
INF: Rayleigh Range              :       24.156 [um]
INF: Eff Focal Spot Area         :       25.460 [um^2]
INF: 1/e Intenity Radius at Focus:        2.847 [um]
INF: Sigma(xp) at Focus          :        2.013 [um]
INF: Sigma(yp) at Focus          :        2.013 [um]
INF: Sigma(zp) at Focus          :      190.967 [um]
INF: Sigma(xp) at z0p_start      :       42.485 [um]
INF: Sigma(yp) at z0p_start      :       42.485 [um]
INF: Sigma(xp) at z0p_stop       :       42.485 [um]
INF: Sigma(yp) at z0p_stop       :       42.485 [um]
INF: Peak Photon Density         :    8.707E+13 [um^-3]
INF: Peak Eta Value              :        0.316
INF: <Eta>     in Focal Vol      :        0.316
INF: Delay of Laser wrt Beam     :        0.000 [um]
INF: Laser Focus Angle           :        3.372 [Deg]
INF:
INF: Calculated Electron Beam Parameters:
INF: -----------------------------------
INF: 1.-Beta of Beam Electron    :    6.012E-11
INF: Gamma   of Beam Electron    :    9.119E+04
INF: Sigma(z) of Electron Density:    6.366E+02 [um]
INF: Peak Electron Density       :    1.596E+03 [um^-3]
INF: <Upsilon> in Focal Vol      :        0.260
INF:
INF: Calculated Parameters for Space-Time-Energy Lattice:
INF: ---------------------------------------------------
INF: Nomin StSi in Time,  Del(t)   :        0.425 [psec]
INF: Nomin StSi in Space, c*Del(t) :      127.311 [um]
INF: Nomin StSi in zp              :      127.311 [um]
INF: Step Size  in xp              :        0.667 [Sigma]
INF: Step Size  in yp              :        0.667 [Sigma]
INF: Nomin StSi in zp              :        0.667 [Sigma]
INF: z0p-Start for Laser           :    -1115.113 [um]
INF: z0p-Stop  for Laser           :     1115.113 [um]
INF: z0 -Start for Beam            :    -1115.113 [um]
INF: z0 -Stop  for Beam            :     1115.113 [um]
INF: Peak Value of Rho*Rho*DV      :    1.042E+19 [um^-3]
INF: Min  Value of Rho*Rho*DV      :    1.042E+17 [um^-3]
INF: Nr of Steps along z,zp (time) :           25
INF: Nr of Energy Bins             :           50
INF: Max Nr of 2nd Steps along Beam:           20
INF:
INF: Calculated Parameters for Coordinate Transformations:
INF: ----------------------------------------------------
INF: Alpha = Angle(Beam,Laser):      197.000 [Deg]
INF: Cos(Alpha)              :       -0.956
INF: Sin(Alpha)              :       -0.292
INF:
TIME-STEP 1 / 25: CPU for Step: 00:00:00, Total: 00:02:58
    <... more similar lines here ...>
TIME-STEP 25 / 25: CPU for Step: 00:00:00, Total: 00:17:36
INF:
INF:  NON-LINEAR QED PROCESSES
INF:     <Energy> |    Photons    |   Electrons  |   Positrons  |     Pairs
```

```
INF: ----------------------------------------------------------------------
INF:    5.000E-01 |   5.3508E+05 |   0.0000E+00 |   0.0000E+00 |   0.0000E+00
INF:    1.500E+00 |   8.7611E+05 |   1.0174E-11 |   5.6281E-17 |   0.0000E+00
INF:    2.500E+00 |   8.5269E+05 |   5.4626E-06 |   5.8449E-11 |   0.0000E+00
    <... more similar lines here ...>
INF:    4.750E+01 |   0.0000E+00 |   0.0000E+00 |   0.0000E+00 |   0.0000E+00
INF:    4.850E+01 |   0.0000E+00 |   0.0000E+00 |   0.0000E+00 |   0.0000E+00
INF:    4.950E+01 |   0.0000E+00 |   0.0000E+00 |   0.0000E+00 |   0.0000E+00
INF: ----------------------------------------------------------------------
INF:     Total    |   2.1278E+07 |   2.1093E+07 |   3.1210E-01 |   3.1210E-01
INF:
INF:   N-Dependence of Non-Linear Compton Scattering:
INF:   N  ------ TOTAL PHOTON -------  ----- TOTAL ELECTRON ------
INF:               Nr        Energy             Nr        Energy
INF: ===========================================================
INF:   1     2.1051E+07    3.0611E+08     2.1051E+07    6.7103E+08
INF:   2     2.1888E+05    5.6318E+06     2.1888E+05    4.4758E+06
INF:   3     6.9290E+03    2.1695E+05     6.9290E+03    1.0238E+05
    <... more similar lines here ...>
INF:   8     1.7658E-02    6.9815E-01     1.7658E-02    1.2119E-01
INF: -----------------------------------------------------------
INF: ALL     2.1278E+07    3.1197E+08     2.1278E+07    6.7561E+08
INF:
INF:   N-Dependence of Breit-Wheeler Process:
INF:   N  ------ TOTAL POSITRONS ----  -------- TOTAL PAIRS ------
INF:               Nr        Energy             Nr        Energy
INF: ===========================================================
INF:   1     0.0000E+00    0.0000E+00     0.0000E+00    0.0000E+00
INF:   2     0.0000E+00    0.0000E+00     0.0000E+00    0.0000E+00
INF:   3     1.8521E-04    3.6892E-03     1.8521E-04    7.3785E-03
    <... more similar lines here ...>
INF:   8     8.2189E-04    1.0060E-02     8.2189E-04    2.0121E-02
INF: -----------------------------------------------------------
INF: ALL     3.1184E-01    4.5818E+00     3.1184E-01    9.1636E+00
INF:
INF:   N-Dependence of Breit-Wheeler Process for Weiz-Will Spectrum:
INF:   N  ------ TOTAL POSITRONS ----  -------- TOTAL PAIRS ------
INF:               Nr        Energy             Nr        Energy
INF: ===========================================================
INF:   1     0.0000E+00    0.0000E+00     0.0000E+00    0.0000E+00
INF:   2     0.0000E+00    0.0000E+00     0.0000E+00    0.0000E+00
INF:   3     0.0000E+00    0.0000E+00     0.0000E+00    0.0000E+00
    <... more similar lines here ...>
INF:   8     2.0555E-05    2.0236E-04     2.0555E-05    4.0472E-04
INF: -----------------------------------------------------------
INF: ALL     2.5372E-04    2.7024E-03     2.5372E-04    5.4047E-03
INF:
INF:  Fast Approx of Total Rates for N=1,2 in NLCS
INF: N=1:    2.088E+07
INF: N=2:    2.271E+05
INF:
INF: Total Nr of Calls to Basic NLCS-Fct: 21711291
INF: Total Nr of Calls to Basic BW  -Fct: 6946003
INF: Total Nr of Calls to Basic Trid-Fct: 142545
INF: END OF NUMERIC INTEGRATION, TOTAL TIME ELLAPSED = 00:17:36
INF: saved histograms to /home/bula/numint/hist/doc_exa.his
```

<ni>.his

contains the histograms booked and filled in `ana_ni.c` in a simple ASCII format. This file can be converted to an HBOOK direct access file (RZ-file) with the name `<ni>.rz` with the following command at the PAW prompt:

```
PAW> exec historz.kum <path><ni>
```

where `<path><ni>` is the path and body (no extention) of the original ASCII-file `<ni>.his`. The two KUIP macro (kumac) files `historz.kum` and `rh.kum` needed for the conversion are installed together with all other program files.

`<nilt>.asc`

stores detailed simulation results of numeric integration lookup table productions in ASCII format. These files are easily transfered between different machines and can be converted to binary format (the actual NILTs) or Ntuples by the programs described in [10].

`<nilt>.bin`

contains the same information as `<nilt>.asc` but in binary format. These files are **NOT** identical to the binary NILTs read or processed by other programs and have not been used so far.

11.3 Setting up the Program Options

Prior to compilation, the program options in `niopt.h` need to be set up. These options select the type of simulation, the processes to be considered, the speed optimizations to be used and the type of analysis calls to be made. Note that some options are not compatible with others, *e.g.* only one of several available options may be selected. A block of preprocessor statements in `nidec.h` checks the consistency of the selected options and tries to avoid the worst conflicts. However, this test is by no means complete and the user should consider it his responsibility to select the program options carefully and in a compatible way. The available options are explained below:

`MIN_PHOTON_NLCS, MAX_PHOTON_NLCS`

Is the minimum and maximum order n (*i.e.* the number of laser photons absorbed at the interaction point) for nonlinear Compton scattering (NLCS).

`MIN_PHOTON_BW, MAX_PHOTON_BW`

Is the minimum and maximum order n (*i.e.* the number of laser photons absorbed at the interaction point) for multiphoton Breit-Wheeler (MPBW) and trident (WWBW) pair production.

`CIRCULAR_POL` or `LINEAR_POL`

Specifies the laser polarization. Obviously, only one of these options can be selected.

`EL_BEAM` or `GA_BEAM`

Selects the type of primary beam, *i.e.* electron beam (`EL_BEAM`) or photon beam (`GA_BEAM`).

Obviously, only one of these options can be selected.

GAMSPE_MONO or GAMSPE_BREMS_SPEC or GAMSPE_LOG_FILE

Specifies the energy spectrum if the primary beam is a photon beam. `GAMSPE_MONO` selects a monochromatic spectrum with energy specified by `ga_ene` in `<ni>.inp`. `GAMSPE_BREMS_SPEC` selects a bremsstrahlung spectrum as described in Sec. 3.3 and defined by the electron beam and foil parameters in `<ni>.inp`. `GAMSPE_LOG_FILE` selects a Compton spectrum previously calculated and saved in a 'log-file' specified by `fn_nilog` in `<ni>.inp`. Obviously, only one of these options can be selected.

FOCUS_ONLY

If this option is selected, the reaction rate is calculated for a single space-time element (STE) at the laser focus ($x' = y' = z' = 0$) and time $t = 0$, *i.e.* when the center of the laser pulse is at the focus. All secondary processes are turned off. The size of the STE is adjusted to $dV \cdot dt \cdot c = 1\mu m^4$ and the density of beam particles is set to $\rho_{\text{beam}} = 1\mu m^{-3}$, independent of other parameters specified in `<ni>.inp`. This option is useful to calculate cross-sections and energy spectra at a fixed value of η.

The following options select the processes considered in the simulation:

P1_NLCS	primary nonlinear Compton scattering,
P1_WWBW	primary multiphoton trident pair production,
P1_KNCS	primary Klein-Nishina approximation,
P1_BW	primary multiphoton Breit-Wheeler pair production,
P1_BS	primary beamstrahlung (static field),
P1_CPP	primary coherent pair production (static field),
P1_WWCPP	primary trident pair production (static field),
P1_NLCS_TOT	fast approximation to primary NLCS ($n = 1, 2$),
P1_BW_TOT	fast approximation to primary MPBW ($n = 1, 2$),
P1_TRID_TOT	fast approximation to primary WWBW,
P1_BS_TOT	fast approximation to primary beamstrahlung (static field),
P2_NLCS	secondary nonlinear Compton scattering,
P2_BW	secondary multiphoton Breit-Wheeler pair production,
P2_WWBW	secondary multiphoton trident pair production,
P2_KNCS	secondary Klein-Nishina approximation,
P2_BS	secondary beamstrahlung (static field),
P2_CPP	secondary coherent pair production (static field),
P2_WWCPP	secondary trident pair production (static field),
P2_CPP_TOT	fast approximation to secondary CPP (static field),

USE_FOCUS_ANGLE

With this option selected, the effective crossing angle between laser photons and beam particles is calculated for each STE as described in Sec. 8.1.

`USE_ELECTRON_SPENDING`

With this option selected, the effective density of beam particles is calculated for each STE as described in Sec. 8.2.

`USE_GAMMA_POLARIZATION`

With this option selected, the polarization of the photon beam is taken into account in the multiphoton Breit-Wheeler pair production process. In the current version of NI, this option is only supported for a linearly polarized laser field.

`USE_ENEDEP_GP` or `USE_FIXED_GP`

Specifies how the polarization of the photon beam is calculated if the polarization dependent MPBW process is used. In the current version of NI, these options are only supported for a linearly polarized laser field. `USE_ENEDEP_GP` selects the energy dependent polarization as calculated by the NLCS process. `USE_FIXED_GP` selects a fixed photon polarization as specified by the variable `ga_pol` in `<ni>.inp`. Obviously, only one of these options can be selected.

`USE_LOOKUP_TABLE`

Selects to generate and use lookup tables (LTs) instead of repeated, explicit calculations of the Bessel- or A_i-functions. The LTs are described in Sec. 10.

`INTERPOLATE_LOOKUP_TABLE`

Selects to use a linear interpolation instead of a simple average between the points in the LT closest to the specified argument.

`USE_BJ2_TABLE` or `USE_BJ2S_TABLE`

Specifies the group of LTs for the Bessel-functions, *i.e.* for a circularly polarized laser field, as defined in Sec. 10.1. `USE_BJ2_TABLE` selects the first group of LTs consisting of $LT^n_{J2}[i]$. `USE_BJ2S_TABLE` selects the second group of LTs consisting of $LT^n_{J2}[i]$ and $LT^n_{J2S}[i]$. Obviously, only one of these options can be selected. Recommended is the second group of LTs.

`BJT_NVAL`

Specifies the dimension D^{LT}_z of the LTs for the Bessel-functions as described in Sec. 10.1.

`USE_A0_TABLE` or `USE_A02_TABLE`

Specifies the group of LTs for the A_i-functions, *i.e.* for a linearly polarized laser field, as defined in Sec. 10.2. `USE_A0_TABLE` selects the first group of LTs consisting of $LT^n_{A0}[i,j]$. `USE_A02_TABLE` selects the second (ϕ-integrated) group of LTs consisting of $LT^n_{A02}[i,j]$, $LT^n_{SA}[i,j]$

and $LT^n_{\sigma' A02}[i,j]$. Obviously, only one of these options can be selected. Recommended is the second group of LTs.

AOT_NVA and AOT_NVB

Specify the dimensions of the LTs for the A_i-functions in the arguments a (D^{LT}_a) and b (D^{LT}_b) as described in Sec. 10.2.

TLT_DIMF_A and TLT_DIMF_B

This are the factors by which the dimensions of the temporary LTs $T^n_{A02}[i,j]$ and $T^n_{SA}[i,j]$ are increased w.r.t. AOT_NVA and AOT_NVB. Note that the temporary LTs are only needed for the second group of LTs selected by USE_A02_TABLE.

NSTEP_NU

Specifies the default number of steps in the ν-integration for the A_i-functions (see Eq. (7) in Sec. 2.2.5). Note that this number of steps can be redefined by the following option.

NSTEP_CYCLE

Specifies the minimum number of steps per order n in the ν-integration for the A_i-functions. This forces the number of steps to be adjusted to the oscillation frequence of $\cos(\ldots - n\nu)$.

AIFCT_ERR_N

Specifies the maximum allowed value per order n for the measures of inaccuracy $\Delta A(n,a,b)$ and $\Delta A_i(n,a,b)$ $(i = 0,1,2)$ as defined in Eq. (14), Sec. 2.2.5. The error tolerance is increased for higher orders up to a maximum value specified by the next parameter. If all three methods described in Sec. 2.2.5 fail to calculate the A_i-functions within the specified error tolerance, the value of $A_i(n,a,b)$ is set to zero.

MAX_AIFCT_ERR

Specifies an upper limit for AIFCT_ERR_N multiplied by the order n. If this product exceeds MAX_AIFCT_ERR, the error tolerance for this order is set to MAX_AIFCT_ERR.

NSTEP_PHI

Specifies the number of steps in the ϕ-integration of the differential reaction rates for a linearly polarized laser (see Sec. 2.3.2 and 2.4.2).

E2NDV_MF_P1_WWBW and E2DV_MF_P1_WWBW

Specifies the two process specific parameters $R_{\eta 2ndV}$ and $R_{\eta ndV}$ needed to speed optimize the calculation of high order P1_WWBW processes (see Sec. 9.3).

E2NDV_MF_P2_NLCS and E2DV_MF_P2_NLCS

Specifies the two process specific parameters $R_{\eta 2ndV}$ and $R_{\eta ndV}$ needed to speed optimize the calculation of high order P2_NLCS processes (see Sec. 9.3).

`E2NDV_MF_P2_BW` and `E2DV_MF_P2_BW`

Specifies the two process specific parameters $R_{\eta 2ndV}$ and $R_{\eta ndV}$ needed to speed optimize the calculation of high order P2_BW processes (see Sec. 9.3).

`E2NDV_MF_P2_WWBW` and `E2DV_MF_P2_WWBW`

Specifies the two process specific parameters $R_{\eta 2ndV}$ and $R_{\eta ndV}$ needed to speed optimize the calculation of high order P2_WWBW processes (see Sec. 9.3).

`ELSP_CUTOFF`

Specifies the parameter E'_{max}, the cutoff energy in the electron spectrum for speed optimizing the secondary NLCS process (see Sec. 9.4.1).

`ETA2_THRESHOLD`

Specifies the parameter $T_{\eta 2}$ which serves as a threshold value for η^2 and determines the range of the photon spectrum considered in speed optimized calculations of higher order secondary NLCS processes (see Sec. 9.4.2).

`N_BW_CUTOFF`

Specifies the parameter R_{BW} which limits the calculation of the primary and secondary MPBW process to orders with a significant contribution to the total yield of e^+e^- pairs (see Sec. 9.5).

`MBLT_MIN`, `MBLT_MAX` and `MBLT_NVAL`

Specify the LTs for modified Bessel-functions used in the simulations for a static field.

The following options specify the processes for which the analysis routine `analyse_stp()` for primary STEs including secondary processes is called:

`ANA_NL_QED_STP`	any nonlinear QED (NLQED) process,
`ANA_NLCS_STP`	nonlinear Compton scattering (NLCS),
`ANA_KN_STP`	Klein-Nishina approximation (KNCS),
`ANA_BW_STP`	Breit-Wheeler pair production (MPBW),
`ANA_WWBW_STP`	trident pair production (WWBW),
`ANA_BS_STP`	beamstrahlung process, static field (BS),
`ANA_CPP_STP`	coherent pair production, static field (CPP),
`ANA_WWCPP_STP`	trident pair production, static field (WWCPP).

The following options specify the processes for which the analysis routine `analyse_stp()` for primary STEs excluding secondary processes is called:

`ANA_NL_QED_STP_P1`	any nonlinear QED (NLQED) process,

ANA_NLCS_STP_P1	nonlinear Compton scattering (NLCS),
ANA_KN_STP_P1	Klein-Nishina approximation (KNCS),
ANA_BW_STP_P1	Breit-Wheeler pair production (MPBW),
ANA_WWBW_STP_P1	trident pair production (WWBW),
ANA_BS_STP_P1	beamstrahlung process, static field (BS),
ANA_CPP_STP_P1	coherent pair production, static field (CPP),
ANA_WWCPP_STP_P1	trident pair production, static field (WWCPP).

The following options specify the processes for which the analysis routine `analyse_stp_p2()` for secondary STEs is called:

ANA_NL_QED_STP_P2	any nonlinear QED (NLQED) process,
ANA_NLCS_STP_P2	nonlinear Compton scattering (NLCS),
ANA_KN_STP_P2	Klein-Nishina approximation (KNCS),
ANA_BW_STP_P2	Breit-Wheeler pair production (MPBW),
ANA_WWBW_STP_P2	trident pair production (WWBW),
ANA_BS_STP_P2	beamstrahlung process, static field (BS),
ANA_CPP_STP_P2	coherent pair production, static field (CPP),
ANA_WWCPP_STP_P2	trident pair production, static field (WWCPP).

The following options specify the processes for which the 'innerst loop' analysis routine `analyse_loop()`is called:

ANA_P1_NLCS_LOOP	primary nonlinear Compton scattering (NLCS),
ANA_P1_KN_LOOP	primary Klein-Nishina approximation (KNCS),
ANA_P1_BW_LOOP	primary Breit-Wheeler pair production (MPBW),
ANA_P1_WWBW_LOOP	primary trident pair production (WWBW),
ANA_P1_BS_LOOP	primary beamstrahlung process, static field (BS),
ANA_P1_CPP_LOOP	primary coherent pair production, static field (CPP),
ANA_P1_WWCPP_LOOP	primary trident pair production, static field (WWCPP),
ANA_P2_NLCS_LOOP	secondary nonlinear Compton scattering (NLCS),
ANA_P2_KN_LOOP	secondary Klein-Nishina approximation (KNCS),
ANA_P2_BW_LOOP	secondary Breit-Wheeler pair production (MPBW),
ANA_P2_WWBW_LOOP	secondary trident pair production (WWBW),
ANA_P2_BS_LOOP	secondary beamstrahlung process, static field (BS),
ANA_P2_CPP_LOOP	secondary coherent pair production, static field (CPP),
ANA_P2_WWCPP_LOOP	secondary trident pair production, static field (WWCPP).

In addition to the options mentioned above, several debugging options for specific parts of the program or selected processes can be selected. With these options active, the program produces additional printout to the screen and the 'log-file'.

11.4 Specifying the Input Parameters

The parameters describing the laser and the particle beams, the space-time grid, the range and bin width of the energy spectra and many other details of the simulation are read by the executable image `ni.exe` from the input file `<ni>.inp` and are described below:

`log_name`

is the path and file-name of the 'log-file' `<ni>.log`.

`hist_name`

is the path and file-name of the histogram file `<ni>.his`.

`la_lam`

is the wavelength λ of the laser light in μm, *i.e.* $\lambda = 2\pi c/\omega$.

`la_diff_fac`

is the ratio $a = A_{\rm eff}/A_0$, *i.e.* the ratio of the effective and diffraction limited focal spot size of the laser as described in Sec. 3.1.

`la_xovy`

is the ratio of $\sigma_{x'}/\sigma_{y'}$, *i.e.* the width of the laser beam in x' and y'. This parameter has not been described so far and allows to simulate an elliptical laser beam.

`x_angle`

is the crossing angle δ between the laser and particle beam axis in degrees.

`la_ene`

is the total energy $E_{\rm laser}$ in the laser pulse in Joule and determines the total number of laser photons by $N_\omega = E_{\rm laser} \cdot \lambda/hc$.

`la_fnr`

is the f-number ($f_\#$) of the optic that focuses the laser beam onto the interaction point (see Sec. 3.1).

`la_fwhm`

is the temporal full-width-at-half-maximum of the laser pulse ($\tau_{\rm laser}$) in ps (see Eq. (102). in Sec. 3.1).

`la_t_off`

is the temporal offset $t_{\rm off}$ between the two beams in ps (see Sec. 3.2).

`la_x_off` and `la_y_off`

are the spatial offsets in x (x_{off}) and y (y_{off}) between the two beams in μm (see Sec. 3).

`el_ene`

is the energy of a beam electron in GeV.

`el_nr`

is the number of electrons per bunch (N_{beam}) in the primary electron beam (see Eq. (103), Sec. 3.2).

`be_sigx` and `be_sigy`

are the width of the primary beam in x and y in units of μm (see Sec. 3.2).

`be_fwhm`

is the temporal full-width-at-half-maximum of the primary beam (τ_{beam}) in ps (see Eq. (104) in Sec. 3.2).

`la_nsigxp`, `la_nsigyp` and `la_nsigzp`

are the parameters $n^{\sigma}_{x'}$, $n^{\sigma}_{y'}$ and $n^{\sigma}_{z'}$ described in Sec. 4. These parameters define the dimensions of the spatial integration volume around the center of the laser pulse in units of Gaussian sigmas.

`la_nstepxp`, `la_nstepyp` and `la_nstepzp`

are the parameters $n^{\Delta}_{x'}$, $n^{\Delta}_{y'}$ and $n^{\Delta}_{z'}$ described in Sec. 4. These parameters define the number of elements in the integration volume along x', y', z'.

`la_rho_step`

is the parameter Δk described in Sec. 9.1 and defines the maximum allowed change in normalized photon density between two steps in z' or t.

`del_z0ovzp`

is the parameter $R^{dt}_{dz'}$ defined in Eq. (108), Sec. 4 and specifies the ratio of the step-size in time and the step-size along z'.

`rrdv_min_frac`

is the parameter $R_{\rho\rho dV}$ described in Sec. 9.2 and is used to exclude STEs with a low reaction yield from the calculations.

`e2dv_min_frac`

is the parameter $F_{\eta 2dV}$ described in Sec. 5 and serves as a criterion to terminate secondary integrations in time. These secondary integrations are used to account for secondary processes

(Sec. 5) and to calculate the effective density of beam particles (Sec. 8.2).

`maxe` and `dele`

are the default upper boundary and bin width in units of GeV of all energy spectra in the simulation. The lower boundary is assumed to be zero. The value of `maxe` should be an integer multiple of `dele` and should be equal or bigger than `el_ene` or `ga_ene`, depending on the type of primary beam selected in `niopt.h`. Note that the spectra for photons and e^+e^- pairs are shifted by half a bin as described in Sec. 7.

`ga_pol`

defines the energy independent polarization state P of the photon beam as defined in Sec. 2.3.2, Eq. (37). Note that this parameter is used only if the laser polarization is linear and the two options `USE_GAMMA_POLARIZATION` and `USE_FIXED_GP` are selected in `niopt.h`.

`ga_ene`

is the energy of a beam photon in GeV.

`ga_nr`

is the number of photons per bunch (N_{beam}) in the primary photon beam (see Eq. (103), Sec. 3.2).

`foil_zzz`, `foil_rho` and `foil_ddd`

are the atomic number, density of atomic nuclei in units of cm^{-3} and thickness in units of μm of a foil. These parameters are used to calculate the bremsstrahlung spectrum of a photon beam produced by an electron beam incident on the foil. The spectrum is calculated according to Eq. (106) in Sec. 3.3. The incident electron beam is characterized by the parameters `el_ene` and `el_nr` described above, and the spatial dimensions of the photon beam are given by `be_sigx`, `be_sigy` and `be_fwhm`. Note that these parameters are used only if the options `GA_BEAM` and `GAMSPE_BREMS_SPEC` are selected in `niopt.h`.

`fn_nilog`

is the path and file-name of a 'log-file' that contains the photon spectrum from nonlinear Compton scattering calculated by a previous simulation. This spectrum characterized the primary photon beam if the options `GA_BEAM` and `GAMSPE_LOG_FILE` are selected in `niopt.h`.

`max_event` and `max_time`

are specific to the routine `do_multi_event()` in `ni.c` and specify the maximum number of collisions to simulate and the maximum amount of CPU time to spend in this multi event simulation.

`sigma_la_ene`, `sigma_la_fnr`, `sigma_la_fwhm` and `sigma_la_t_off`, `sigma_la_x_off`, `sigma_la_y_off`

are specific to the routine `do_multi_event()` in `ni.c` and specify the widths of the Gaussian distributions describing the laser parameters for multi-event simulations. The mean value of these distributions is given by the corresponding parameters described above. The actual laser parameters for a simulation are then chosen randomly according to the Gaussian distributions.

An example of a input file is listed below:

```
                                /* FILE-NAMES */
log_name     log/doc_exa.log    /* log-file       with path */
hist_name   hist/doc_exa.his    /* histogram-file with path */

                                /* FOR LASER */
la_lam            0.527         /* wavelength of laser photons     [um]    */
la_diff_fac       4.0           /* ratio A_eff(0)/A_diff_limit(0)          */
la_xovy           1.0           /* ratio la_sigx0p / la_sigy0p             */
x_angle          17.0           /* X-ing angle betw beam and laser [Deg]   */
la_ene            0.400         /* energy of laser pulse           [Joule] */
la_fnr            6.0           /* f-number of focusing optics             */
la_fwhm           1.5           /* FWHM of laser intensity in t    [psec]  */
la_t_off          0.0           /* delay of laser wrt beam bunch [psec]    */
la_x_off          0.0           /* x-offset of laser beam wrt e- beam [um] */
la_y_off          0.0           /* y-offset of laser beam wrt e- beam [um] */

                                /* FOR ELECTRON BEAM */
el_ene           46.6           /* Energy of incoming electron beam [GeV]  */
el_nr           1.0E10           /* Nr of Electrons in one bunch            */

                                /* FOR ELECTRON/GAMMA BEAM */
be_sigx          25.0           /* Sigma of beam density in x   [um]   */
be_sigy          25.0           /* Sigma of beam density in y   [um]   */
be_fwhm           5.0           /* FWHM  of beam density in t   [psec] */

                                /* FOR SPACE-TIME LATTICE */
la_nsigxp         3.0           /* spatial range around center of laser */
la_nsigyp         3.0           /* considered in calculation, in units  */
la_nsigzp         3.0           /* of sigmas                            */
la_nstepxp          9           /* Nr of steps betw +- la_nsigxp */
la_nstepyp          9           /* Nr of steps betw +- la_nsigyp */
la_nstepzp          9           /* Nr of steps betw +- la_nsigzp */
la_rho_step       0.2           /* Photon Dens Step-Size around focus ]0,1[ */
del_z0ovzp        1.0           /* Step-Size c*del(t), in units of         */
                                /* 2*la_nsigzp*la_sigz0p/la_nstepzp,       */
                                /* i.e. the step size in zp for spatial int */
rrdv_min_frac     1.0E-2        /* consider STP only if be_rho*la_rho*dvol  */
                                /* is > rrdv_min_frac * 'value at peak'     */
e2dv_min_frac     1.0E-3        /* stop integration along beam-direction           */
                                /* (for sec proc and El dens calculation)          */
                                /* if eta^2*dVol < e2dv_min_frac * eta2n_dv_peak[1] */
                                /* i.e. if eta^2*dVol has droped below the         */
                                /* min. fraction of the peak value for all STE     */

                                /* FOR ENERGY BINNING */
maxe             50.0           /* maximum energy of scattered particles [GeV] */
dele              1.0           /* Bin-Width [GeV] */

                                /* FOR GAMMA POLARIZATION */
                                /* effective if USE_GAMMA_POLARIZATION is selected  */
                                /* applies to complete gamma-spectrum (energy-indep)*/
```

```
ga_pol            1.0         /* LINEAR POL LASER: 1=parallel      to laser field */
                              /*                   0=perpendicular to laser field */


                              /* FOR MONOENERGETIC GAMMA BEAM */
ga_ene          250.0        /* Energy of incoming gamma beam [GeV] */
ga_nr           5.0E9         /* Nr of gammas in one bunch           */

                              /* FOR GAMMA SPECTRUM */
foil_zzz         13.0         /* Z or foil material                   */
foil_rho          6.03E22     /* density of foil nuclei       [cm^-3] */
foil_ddd        100.0         /* thickness of foil            [um]    */
fn_nilog   log/gc400.log      /* name of ni.log-file to read gamma-spectrum */

                              /* for multiple event simulation */
max_event        5000         /* max nr of events to simulate  */
max_time          600         /* max time to spend (sec)       */
sigma_la_ene      0.250       /* sigma of laser energy [Joule] */
sigma_la_fnr      6.0         /* sigma of laser f-number       */
sigma_la_fwhm     2.0         /* sigma of laser FWHM   [psec]  */
sigma_la_t_off    4.0         /* sigma of laser delay  [psec]  */
sigma_la_x_off    0.0         /* sigma of laser x-offset [um]  */
sigma_la_y_off    0.0         /* sigma of laser y-offset [um]  */
```

11.5 Source Code and Program Installation

The program is installed on the SLAC UNIX platform in the directory

`/usr/local/e144/user/numint.`

The complete source code is also available in compressed format for the DOS operation system at

`/usr/local/e144/user/numint/source/ni_dos.zip`

and for the UNIX or LINUX operating systems at

`/usr/local/e144/user/numint/source/ni_unix.zip`

These compressed files also contain the utility programs for numeric integration lookup tables (NILTs) as described in [10]

To install and run the program at another location on a UNIX or LINUX platform, follow the steps below:

1. Copy the compressed file `ni_unix.zip` to the new location and uncompress the file, *i.e.* `unzip -La ni_unix.zip`. The option `-L` converts all file names to lower case and `-a` treats all files as text-files.
2. Create the subdirectories `./log`, `./hist` and `./lt`.
3. Copy the file `environ.sta` to `environ.h`.
4. Edit the file `environ.h`, select the type of operating system and set the path names to the program files.

5. Edit the file `makefile` and set the path names, compiler name and compiler options.
6. Specify the simulation parameters and analysis options you want by setting up the files `ni.c`, `ana_ni.c`, `niopt.h` and `ni.inp` as described in the previous sections.
7. Compile and link the program with `make ni`.
8. That's it, run the program and have fun ...

Note that the program was developed on a DOS PC with the Microsoft C/C++ compiler and the source code contains two features that are not ANSI-C compatible, namely comments are sometimes preceded by `//`, *i.e.* a C++ convention, and nested preprocessor directives are often indented to improve the readability of the code. The GNU C-compiler `gcc` is compatible with these extensions, but other compilers may not be. To clean source files from these extensions, the program `prep.c` is provided and, after compiling and linking with `gcc prep.c -o prep`, can be used as

```
prep <fnin> <fnout>
```

where `<fnin>` is the name of the original source file and `<fnout>` is the name of the 'cleaned', ANSI-C compatible source file. The shell script `niprep.ux` shows an example of using `prep` to process all source files. Both `prep.c` and `niprep.ux` are included in the compressed file `ni_unix.zip`.

To install and run the program on a DOS machine with the Microsoft C/C++ compiler, Vers. 8 or higher installed, follow the steps below :

1. Copy the compressed file `ni_dos.zip` to the top directory, *e.g.* `C:\`.
2. Create the directories `C:\numint` and `C:\dev` and add them to your INCLUDE-path (usually in `autoexec.bat`).
3. Uncompress the file, *i.e.* `pkunzip -d -o ni_dos.zip`. Note that some of the program files are extracted to `C:\numint` and others to `C:\dev`.
   (In principle, all files can go to the same directory. However, in that case the files `ni.bat` and `environ.h` need to be adjusted.)
4. Create the subdirectories `C:\numint\log`, `C:\numint\hist` and `C:\numint\lt`.
5. Copy the file `environ.sta` to `environ.h`.
6. Edit the file `C:\dev\environ.h` and select the MS-DOS operating system. Make sure the path name `NI_HOME` is set to `C:\numint\` and `DAQ_HOME` is set to `C:\dev\`.
7. Specify the simulation parameters and analysis options you want by setting up the files `ni.c`, `ana_ni.c`, `niopt.h` and `ni.inp` as described in the previous sections.
8. Compile and link the program by running the 'bat-file' `ni.bat` (sorry, no make-file for DOS).
9. That's it, run the program and have fun ...

References

[1] A.I. Nikishov and V.I. Ritus, 'Quantum Processes in the Field of a Plane electromagnetic Wave and in a Constant Field. I,' Sov. Phys. JETP **19**, 529 (1964).

[2] N.B. Narozhny *et al.*, 'Quantum Processes in the Field of a Circularly Polarized Electromagnetic Wave,' Sov. Phys. JETP **20**, 622 (1965).

[3] A.I. Nikishov and V.I. Ritus, 'Nonlinear Effects in Compton Scattering and Pair Production Owing to Absorption of Several Photons,' **20**, 757 (1965).

[4] K.T. McDonald, 'Proposal for Experimental Studies of Nonlinear Quantum Electrodynamics,' Princeton U. preprint DOE/ER/3072-38 (Sept. 1986).

[5] K. Shmakov, privat communication, 1997.

[6] C. Bula and K.T. McDonald, 'E-144: The Weizsaćker-Williams Approximation to Trident Production in Electron-Photon Collisions', E-144 internal note, Jan. 1997, http://www.slac.stanford.edu/exp/e144/ps/trident.ps.

[7] D.D. Meyerhofer, 'Summary of Gaussian Focusing', E-144 internal note, June 1994.

[8] D.D. Meyerhofer, 'Non-diffraction Limited Focusing', E-144 internal note, Feb. 1995.

[9] H.W. Koch and J.W. Motz, Rev. Mod. Phys. **31**, 920 (1959).

[10] C. Bula, 'Production and Usage of Numeric Integration Lookup Tables', E-144 internal note, to be written, http://www.slac.stanford.edu/exp/e144/ps/nilt.ps.